Removal of Phosphorus from Domestic Sewage by a Constructed Wetland Coupled Microbial Fuel Cell System

Shuang Yu
North China University of Science and Technology
Peng Dou
Beijing Water Science and Technology Institute
Yue Yin
North China University of Science and Technology
Peijing Wang
Beijing Water Science and Technology Institute
Hao Wang (wanghao@ncst.edu.cn)
North China University of Science and Technology
Jinlong Han
North China University of Science and Technology
Duo Xu
North China University of Science and Technology

Research Article

Keywords: constructed wetland, domestic sewage, electricity production, microbial fuel cell, total phosphorus

Posted Date: July 26th, 2021

DOI: https://doi.org/10.21203/rs.3.rs-666622/v1

Abstract

A constructed wetland (CW) coupled microbial fuel cell (MFC) system that treats wastewater and generates electricity was constructed. The total phosphorus in the simulated domestic sewage was used as the treatment target, and the optimal phosphorus removal effect and electricity generation were determined by comparing the changes in substrates, hydraulic retention times, and microorganisms. The mechanism underlying phosphorus removal was also analyzed. The experimental results showed that the best removal efficiencies of the two CW-MFC systems that used magnesia and garnet as substrates were 80.3% and 92.4%, respectively. Phosphorus removal by the garnet matrix mainly depends on a complex adsorption process whereas the magnesia system relies on ion exchange reactions. The CW-MFC system can also generate electricity. The highest output voltage and stable voltage of the garnet system were both higher than those of the magnesia system. The maximum stable voltage of the garnet device was 500 mV, while that of the magnesia device was 290 mV. The microorganisms in the soil and in the electrode within the wetland sediments also substantially changed, indicating that microorganisms positively respond to the removal of organic matter and power generation. Combining the advantages of constructed wetlands and microbial fuel cells also improves phosphorus removal in the coupled system. Therefore, when studying a CW-MFC system, the selection of electrode materials, matrix, and system structure should be taken into account in order to find a method that will improve the power generation capacity of the system and remove phosphorus.

1 Introduction

The rapid development of economic construction has meant that water pollution in China has meant that wastewater treatment has become an important problem and the aquatic ecology has been seriously damaged (Zhou et al. 2020; Wen et al. 2021). It has become a particular problem for domestic wastewater and industrial wastewater drainage, and agricultural irrigation. Industrial wastewater not only consumes a large amount of water but also has a low reuse rate. Agricultural irrigation water and sewage discharges contain large amounts of pesticides and fertilizers which seep from the soil to the groundwater resulting in serious degradation of the aquatic environment (Mander et al. 2021). Studies have shown that a constructed wetland (CW) coupled microbial fuel cell (CW-MFC) system can generate electrical energy and treat sewage (Xu et al. 2021). It can not only enhance the electricity generation performance of the MFC, but also improve organic matter removal efficiency. Indeed, CW-MFC is a new sewage treatment system with very promising development prospects (Patel et al. 2021;). However, there are still many operational problems to be solved.

Constructed wetlands are used to treat sewage and sludge by combining the effects of soil, plants, microorganisms, and artificial media (Fhl et al. 2020; Overbeek et al. 2020; Tang et al. 2020). They have the advantages of low construction cost and good treatment effect, etc. and are widely used (Schierano et al. 2020; Deng et al. 2020). A CW is a natural wetland system with manual monitoring and control. The first constructed wetland system in the world appeared in the United Kingdom and has been running for 90 years since 1903. Subsequently, a large number of researchers began to study the CW system. Today

CWs are highly popular around the world (Walaszek et al. 2018; Li et al. 2018; Liang et al. 2020). They use the biological, physical, and chemical functions of the microbial-plant-matrix to purify sewage, and the nutrients in water and sewage also improve plant growth (Rodrigo et al. 2018). Constructed wetlands are highly efficient at treating rainfall and snowfall, domestic sewage, industrial wastewater, and agricultural irrigation wastewater (Tunsiper 2020; Uusheimo et al. 2018; Pelissari et al. 2017).

Microbial fuel cells (MFCs) are a new type of energy saving device. They are a biochemical system that uses microorganisms to degrade organic matter and generate electric energy (Wang et al. 2020; Xu et al. 2019; Wu et al. 2020). Microbes in the system consume organic matter and convert chemical energy into electricity (Niu et al. 2020; Hai et al. 2020). The organic materials in the anode are degraded by microorganisms in the anaerobic environment, and this degradation releases electrons and protons from the anode. The protons enter the cathode through the proton exchange membrane. They are transferred outward from the anode through the medium and the anode is connected to the cathode by an external circuit (Ahmadpour et al. 2020). In recent years, studies have shown that the MFC system has a good removal effect for refractory organic matter and can use the easily degradable organic matter as a matrix to generate electricity (Lim et al. 2021; González et al. 2020; Colares et al. 2020).

A two-compartment MFC was the first MFC to be successfully studied because it is easier to study the mechanism underlying electricity generation and to isolate and determine the function of electricity-producing bacteria (Rout et al. 2020). Therefore, a two-compartment MFC is the most widely used in MFC research and development. The operating principle of an sediment microbial fuel cells (SMFC) is to use organic matter in the sediment to produce electrons that can subsequently remove easily oxidized organic matter in the sediment and degrade some difficult to degrade organic compounds, such as aromatic hydrocarbons and phenolic compounds (Yan et al. 2017; Liu et al. 2019). Studies have found that an SMFC running for 5 months can reduce the total organic matter content in the sediment by 21.9% and the content of easily oxidized organic matter by 32.7% (Yang et al. 2020).

In recent years, studies have shown that cyanobacteria have nanowires, which theoretically suggests that they can directly transfer electrons (Abazarian et al. 2020). Deshamphelaire et al. successfully constructed a rice MFC system by placing the electrode on a rice root and using the root-microbial-electrochemical action. After operation, the results showed that the output power of the rice MFC system was 0.1 W/m^2, which was seven times of that of the SMFC group system without rice. This indicates that plants play an active role in the survival and reproduction of microorganisms.

The CW-MFC system is a new sewage treatment system (Gupta et al. 2020; Zhang et al. 2017). A CW-MFC coupling system can generate electric energy while treating sewage. It enhances the power generation performance of an MFC and improves the organic matter removal efficiency. It is a new sewage treatment system with very promising development prospects (Xu et al. 2018; Lei et al. 2018). Its unique operating principle means that it can generate energy at the same time as treating wastewater and has broad development prospects (Oon et al. 2018; Ge et al. 2019).

Lix et al. (2012) constructed an MFC in a CW system and successfully created the first vertical flow constructed wetland microbial fuel cell coupling system. The experimental results showed that when the external resistance was 1000, the maximum chemical oxygen demand (COD) removal rate could reach 94.4%, the maximum current density was 2 A/m^3, and the maximum power density was 0.149 W/m^3 when the simulated sewage was manually prepared with glucose as substrate. The high concentration of organic pollutants in sewage and the increase in the COD removal rate improved electricity generation performance. The maximum current density and maximum power density of the MFC in the system were 69.75 mA/m^2 and 15.73 mW/m^2, respectively, and the COD concentration in the influent was 1000 mg/L at this point.

Phosphorus is the key nutrient that causes water eutrophication (Wang et al. 2018). In recent years, there has been a considerable increase in research on phosphorus removal by CW systems in China and elsewhere (Ma et al. 2020; Nguyen et al. 2020). In this study, the CW-MFC system was taken as the research object, and CW-MFC wetland substrate selection, operating conditions, and electricity generation performance were investigated. Firstly, matrices with a good phosphorus removal effects were screened out, and the influence of their related properties on phosphorus removal and electricity generation performance were studied. The CW-MFC system can effectively remove phosphorus while improving electricity generation. The changes to and the roles of microorganisms during phosphorus removal in the CW-MFC system are discussed, and the mechanism driving phosphorus migration, transformation, and removal in the CW-MFC system was analyzed. The results provide theoretical and technical support for the popularization and application of CW-MFC systems to remove phosphorus.

2 Methods And Materials

2.1 Experimental device

In this experiment, two types of CW-MFC devices were set up and different fillers were added. The two devices had a height of 40 cm, a length of 34 cm, and a width of 18 cm. The total volume of the apparatus was 20 L and the effective water storage volume after adding fillers was about 6 L (Fig. 1).

Sampling ports were set at 9, 18, 27, and 36 cm from the bottom along the direction of the cylinder. There was a water inlet at the bottom of the device and the valve was connected to the peristaltic pump using a silicone tube. From bottom to top, the device was divided into four areas, namely the lower matrix (12 cm), anode area (8 cm), upper matrix (12 cm), and air cathode area (5 cm). Two aquatic plants were planted in the top layer. The CW-MFC system was connected to a 1000 Ω resistor, and the cathode and anode were connected via a copper wire to form a closed loop. The voltage generated was automatically measured by the data collector.

2.2 Selection of experimental materials

2.2.1 Matrix selection

The matrix plays a major role in the removal of phosphorus by the CW-MFC system. The phosphorus removal mechanism is mainly adsorption and precipitation. Studies have shown that during the phosphorus removal process in CW systems, the phosphorus removal efficiency of the substrate is much higher than that of plants and microorganisms, and the removal ratio can be as high as 70–87%. Therefore, the selection of a suitable substrate has an important impact on the phosphorus removal efficiency of the whole system. After comprehensive consideration and analysis of the treatment effect and economic factors, it was decided to use magnesia and garnet as the substrates because they are rich in metal ions and are relatively low cost. The 3–5 mm uniform magnesia and garnet were cleaned and thoroughly dried, and then placed into two of the devices which became the control group.

2.2.2 Plant selection

Plants are an important part of the microbial fuel cell system in CWs. The water plants *Eichhornia crassipes* and *Hemerocallis* were selected because they have a strong ability to remove phosphorus. The *Eichhornia crassipes* was bought in a flower market and the *Hemerocallis* was taken from the campus of the North China University of Science and Technology. In the two sets of devices, five uniformly sized *Eichhornia crassipes* and five *Hemerocallis* plants were placed in the middle of the air cathode and the upper substrate at the same density.

2.2.3 Selection of activated sludge

The activated sludge was taken from the biochemical pond of the Caofeidian New Town Sewage Treatment Plant in Tangshan City, China. The treatment plant has a daily treatment capacity of 20,000 cubic meters per day. The equipment at the plant includes: (1) newly added fixed fillers in the retort tank; (2) a newly built denitrification deep bed filter and an intermediate lift pump room; and (3) new equipment in the sludge dewatering machine room. After the sludge is retrieved, it is subjected to anaerobic treatment in the laboratory, cultured for 2 weeks, and then washed with deionized water to remove residual COD. The waste is then inoculated into the reactor cathode and anode activated carbon.

2.2.4 Electrode selection

In this experiment, both the cathode and anode used activated carbon as the electrode material. Activated carbon has a large specific surface area, good conductivity and adsorption capacity, and is widely used as an electrode material because it is a convenient material and moderately priced. Before use, it needs to be washed and soaked with distilled water at least three times, then soaked with 1 mol NaOH and HCl for 24 h, and finally washed with distilled water more than five times to remove surface pollutants and impurities. A three layer stainless steel mesh was placed in the middle of the activated carbon to increase the electrical conductivity. A part of the cathode was exposed to the air to form an air cathode and the stainless steel mesh was connected to it with the copper wire to form a loop.

2.2.5 Chemicals

The chemicals needed for this experiment were potassium dihydrogen phosphate, glucose, ammonium chloride, potassium dichromate, silver sulfate, mercury sulfate, ascorbic acid, ammonium molybdate,

potassium antimony tartrate, sulfuric acid, sodium hydroxide, and hydrochloric acid, A FastDNA Spin kit for soil was used to extract the soil microbial genomic DNA.

2.2.6 Experimental equipment

The main experimental equipment used included pH test paper, qualitative filter paper, measuring cylinders, a thermometer, funnels, volumetric flasks, digestion tubes, brown bottles, 50 mL colorimetric tubes with stoppers, cuvettes, test tubes, conical flasks, and beakers. The main instruments and equipment used in the experiment is shown in Table 1:

Table 1
List of the main instruments and equipment used in the experiment

Equipment name	Model	Manufacturer
Electronic analytical balance	FA2204B	Shanghai Jingke Tianmei Scientific Instrument Co., Ltd.
Smart digester	CM-05	Beijing Shuanghui Jingcheng Electronic Products Co., Ltd.
Electric heating constant Temperature blast drying oven	DHG-9101	Jintan Medical Instrument Factory
Magnetic stirrer	BBC-7X	Hangzhou Changsheng Group
UV-visible Spectrophotometer	T6	Beijing Puxi General Instrument Co., Ltd.
Peristaltic pump	YZ15	Baoding Refu Fluid Technology Co., Ltd.
Infrared spectrometer	IRAffinity-1s	Japan Shimadzu Corporation
pH meter	PHS-3C	Shanghai Precision Scientific Instrument Co., Ltd.
Ultra pure water machine	GWA-UN	Beijing Universal
Water bath constant temperature oscillator	THZ-82	Jiangsu Ronghua Experimental Equipment Co., Ltd.
Multi-channel data acquisition system	PISO813	Shenzhen Changxin Automation Equipment Co., Ltd.

2.2.7 Water used in the experiment

The experimental water was tap water because it simulates actual domestic sewage. The theoretical water quality index is shown in Table 2 and the main compounds in the water are shown in Table 3. A

trace element solution (1 mL) was added to each liter of water in the simulated sewage. The compounds and their concentrations in the trace element solution are shown in Table 4.

Table 2
Simulated sewage water quality index

Number	Total phosphorus concentration mg/L	COD mg/L	Ammonia nitrogen concentration mg/L
1	1	230	5
2	2	460	10
3	3	690	15
4	5	1000	25

Table 3
Simulated sewage formula

Number	Glucose (g)	Potassium dihydrogen Phosphate(g)	Ammonium chloride (g)
1	5.4	0.0931	0.456
2	10.5	0.1862	0.9
3	15.7	0.2780	1.368
4	22	0.46	1.9

Table 4
Trace element concentration

Drug	Concentration (mg/L)
$(NH4)_6Mo_7O_{24}$	0.0011
H_3BO_3	0.0015
$FeSO_4$	0.004
$CuSO_4$	0.0015
$MnCl_2$	0.005
$ZnSO_4$	0.022
$CoCl_2$	0.0016
$CaCl_2$	0.0052

2.3 Experimental procedure

The experimental period lasted seven months, and the first phase consisted of commissioning the experiment. The plants grown in the air cathode and the upper substrate simulated the phosphorous sewage system. The trace element nutrient solution was added to the water and then the water was pumped by a peristaltic sewage pump into the device through the bottom inlet, Then domestication of the activated sludge and cultivation of aquatic plants began, and the COD and voltage of the effluent were monitored and recorded every day. When the COD of the effluent gradually decreases and the electricity generation voltage reaches a relatively stable state, it means that the microorganisms are successfully attached to the membrane and acclimation of activated sludge is complete. At this point, wastewater containing a low concentration of phosphorus can be introduced to start the formal experiment.

In the second stage, the CW-MFCs containing the magnesia or garnet were operated simultaneously. First, domestic sewage with a total phosphorus concentration of 1 mg/L and a COD of 230 mg/L was injected into the device, 15 mL water samples were removed from the four outlets every 24 h, and the total phosphorus and COD concentrations in the water were measured after filtration through a filter membrane. The hydraulic retention time (HRT) was set to 5 days and the experiment was repeated three times. After running for one month, the total phosphorus concentration was increased to 2 mg/L, 3 mg/L, and 5 mg/L, the concentration was increased to 460 mg/L, 690 mg/L, and 1000 mg/L, and the above operation was repeated. Then, the different effects of the magnesia and garnet substrates on phosphorus removal were compared, and the effects of the different pollutant concentrations on the removal rate and the cathode anode and substrate phosphorus removal efficiencies were tested. During this phase, the voltages generated by the CW-MFCs were automatically recorded by a multi-channel data collector. The

MFC component was removed in the third stage to leave just the CW component and the second stage experiment was repeated to compare the pollutant removal effect of the CW and CW-MFC systems.

Soil samples were collected from the 0 ~ 10 cm and 10 ~ 30 cm layers of the CW sediments and marked as D10 and D30 respectively. A Fast DNA Spin kit for soil was used to extract soil microbial genomic DNA. A 0.5 g soil sample was weighed and the total soil microbial DNA was extracted and dissolved in 100 μL sterile TE buffer. The DNA concentration was determined by a microultraviolet spectrophotometer and DNA integrity was analyzed by 1% agarose gel electrophoresis. The soil DNA was stored in a − 80 ℃ freezer for further analysis.

The soil DNA was amplified with bacterial universal primers 515F (5' -GTGCCAGCMGCCGCGG-3 ') and 907R (5' -CCGTCAATTCMTTTRACTTT-3 '). The amplification system contained 25 μL Premix TaqTM, 1.0 μL 515F primer, 1.0 μL 907R primer, and 2.0 μL 10 times diluted DNA template. Then, sterilized double-distilled water was added so that the final volume of the reaction system was 50 μL. Each PCR bacterium product was assigned a negative control of sterilized double-distilled water. The PCR amplification conditions were as follows: 94 ℃, 5 min; 94 ℃, 30 s; 55 ℃, 30 s; and 72 ℃, 45 s over 30 cycles with a final 72 ℃ for 10 min. The amplification products were purified and each sample was dissolved in 40 μL elution buffer. Then, the DNA concentration was determined again. The different samples were mixed in equal masses, an AxyPrep DNA gel recovery kit was used for gum purification after it was dissolved in 30 μL DNAase-free H_2O. The purified PCR products were detected by 1.8% agarose gel electrophoresis and the concentration of the purified PCR products was determined. They were then sequenced on an Illumina MiSeq sequencing platform.

2.4 Measurement and calculation

Chemical oxygen demand reflects the degree of water pollution by reducing substances. The COD was measured using potassium dichromate rapid digestion spectrophotometry and the COD removal rate was calculated using the formula:

$$COD_{\text{removal rate}} = \frac{COD_{\text{in}} - COD_{\text{out}}}{\text{COD}_{\text{in}}}$$

Molybdenum antimony spectrophotometry was used to measure total phosphorus. Briefly, phosphate standard solutions (0, 0.5, 1, 3, 5, 10, and 15 mL) were poured into seven separate 50 mL colorimetric tubes with stoppers and distilled water was added to the 50 mL mark. Then, 1 mL 10% ascorbic acid solution was added to each colorimetric tube followed by 2 mL molybdate solution after 30 s. The tubes were mixed well and left to stand for 10 min. A spectrophotometer was used to measure the absorbance at 700 mm wavelength. Then, the pattern for the blank tube was subtracted from the results to create the standard curve for total phosphorus concentration. Following this, an appropriate amount of each sample was filtered using a filter membrane. After digestion, the above method was used to develop the color and measure the absorbance, and the total phosphorus concentration was obtained from the standard curve.

Voltage includes open-circuit voltage and closed-circuit voltage. In this experiment, the CW-MFC system was connected to a 1000 Ω resistor, and the cathode and anode were connected via a copper wire to form a closed loop. The data were collected every 10 min and the voltage generated was determined by equipment installed in the computer. The collector automatically recorded that this voltage was the closed-circuit voltage. Then, the cathode and anode were disconnected from the resistor and the cathode and anode wires were connected to form a closed circuit, which allowed the open-circuit voltage to be measured. The saturated calomel electrode was then connected to the open cathode and anode so that the cathode or anode potentials could be measured. The current was determined from the voltage and external resistance and calculated according to Ohm's law.

When the external resistance changes within a certain range, the current density and the output voltage will form a curve relationship. This curve is the polarization curve and the relationship curve formed by the current and power density is the power density curve. When the system was running stably, an external resistance of 10–5000 Ω was set up between the cathode and anode so that the output voltage at both ends of the external resistance could be measured and the system polarization curve and power density curve could be obtained. These two curves were then fitted into an equation.

Quantitative PCR labeling was undertaken using universal primers 515F/907R, and general purpose primer amplification gene cloning was used to build the gene library. The library contained the target genes in the nutrient solution. The plasmids containing the genes were subjected to plasmid purification and the plasmid concentration was determined according to the Moore constant calculation target gene copy number. Then, the plasmids were serially diluted by eight orders of magnitude to obtain the standard curves for the genes.

Three kinds of substrates were selected for the control test, namely cordierite, magnesia, and garnet. Before use, they were cleaned, dried, crushed, and screened. Then 8 g pieces of each substrate were placed in a 250 mL conical flask with a stopper, and 200 mL solutions containing 10, 20, 30, 40, 50, 60, and 70 mg/L potassium dihydrogen phosphate at neutral pH were added to the flask. The flask was placed in a constant temperature oscillating chamber at 25℃ and 125 r/min for 24 h to equilibrate. The absorbance was determined by a spectrophotometer. The phosphorus concentration of the solution was obtained by comparing the standard curve with the spectrophotometric method. The equilibrium adsorption amount for phosphorus was calculated by the following formula.

3 Results And Discussion

3.1 Analysis of the system phosphorus removal effect

3.1.1 Total phosphorus removal efficiency at different pollutant concentrations

In this group of experiments, four different influent phosphorus concentrations were used, namely 1, 2, 3, and 5 mg/L. The COD concentrations were 230, 460, 690, and 1000 mg/L, respectively, the total hydraulic retention time was 5 days, and sampling took place once every 24 h. After the samples had been filtered, the total phosphorus concentration in the top outlet solution was determined and the effects of the magnesia and garnet treatments at different influent pollutant concentrations were compared. The garnet device was referred to as device I, and the magnesia device was called device II.

Figure 2 shows that when the phosphorus concentration of the influent water was 1, 2, 3, and 5 mg/L the total phosphorus removal rate of device I reached 92.4%, 87.35%, 82%, and 78%, respectively, and the phosphorus removal rate for device II reached 80.3%, 77.9%, 75%, and 67%, respectively. It can be seen that the treatment effect of device I is stronger than that of device II. Furthermore, as the hydraulic retention time increases, the simulated domestic sewage treatment efficiency at the different influent phosphorus concentrations also shows an upward trend. When the hydraulic retention time is 1 day, the removal efficiency shows a rapid increase and the removal rates of the two devices reach about half of the total removal rate. The removal rate increased rapidly from the second day to the third day, but then the removal rate only increased slightly. This suggests that total phosphorus removal by the system mainly depends on filtration and adsorption by the matrix. The removal rate increase slowed as the matrix became saturated after a certain point. The total phosphorus removal rate also decreased as the influent pollutant concentration increased. The sewage treatment effect was optimal when the influent pollutant was 1 mg/L. In general, an increase in influent pollutant concentration and long-term operation of the system could easily saturate the matrix. However, this system overflows with phosphate ions and then re-adsorbs and degrades them.

3.1.2 Comparison between the phosphorus removal effects of the CW-MFC and CW systems

After the completion of the second phase of the experiment, the microbial fuel cell was disconnected and the external resistor, the cathode, and the anode were removed, which made the system into a separate CW system that still used the operation mode of water inlet and outlet from the bottom. The water phosphorus concentrations were 1, 2, 3, and 5 mg/L, the total hydraulic retention time was 5 days, and the system was sampled every 24 h. After filtration, the total phosphorus concentration in the uppermost water outlet solution was determined and compared with the phosphorus removal effects by the CW-MFC system.

Figure 3 is a comparison of the phosphorus removal effect between the CW-MFC system based on the two substrates and the CW system. It can be seen that, for both substrates, phosphorus removal by the CW-MFC system is better than that of the CW system. The difference between the two systems was smallest when the influent concentration was 1 mg/L. Furthermore, removal by the garnet based system is better than that of the magnesia-based system. This shows that the type of MFC system used has an impact on the removal of total phosphorus. In addition, electrolysis by the system and the action of microorganisms, such as phosphorus accumulating bacteria and phosphorus phagophores, also have an

impact on the removal of phosphorus. The phosphorus removal effect of the garnet matrix is stronger than that of the magnesia matrix. The decrease in the treatment effect at the higher pollutant concentrations was probably due to the matrices becoming saturated.

3.2 Analysis of the COD removal effect

3.2.1 COD removal rate at different pollutant concentrations

There were four different influent COD concentrations in this experiment: 230, 460, 690, and 1000 mg/L. The total hydraulic retention time was 5 days, sampling took place every 24 h, and the samples were filtered before they were analyzed. The total phosphorus concentration in the uppermost water outlet solution was compared with the COD removal effect due magnesia and garnet at different influent pollutant concentrations as the hydraulic retention time increased. As above, the device with garnet as the matrix is device I, and the device with magnesia as the matrix is device II.

When the influent COD concentration was 230, 460, 690, and 1000 mg/L, the COD removal rates were 91.56%, 88.73%, 80% for device I and 73%, and 93.74%, 94.21%, 83.5%, and 85.1% for device II, respectively. The treatment effect of device II was stronger than that of device I. Between 0 h and 48 h HRT, the treatment efficiency of the simulated domestic sewage device showed a rapid upward trend at all influent COD concentrations and the removal rate of the two devices approximately approached the optimal removal rate. Between 48 and 72 h, the COD concentration in the devices suddenly increased and the removal rate decreased. After 72 h, the removal rate showed a linear increase again, finally achieving the optimal removal rate at 120 h. The devices also reached approximately their optimal treatment rate when the lowest influent COD concentration was added during the first stage. As the concentration of the influent pollutants increased, the treatment efficiency gradually decreased. This suggests that the different removal effects shown by the devices may be because the magnesia consumes more organic matter in the anodic oxidation-reduction reaction. The fluctuation in the removal effect of the systems shows that the optimal system reaction time is 48 h, and new pollutants will appear in the system after 48 h.

3.2.2 Comparison of the COD removal effect between the CW-MFC system and CW system

After completion of the second phase of the experiment, the microbial fuel cell was removed and the connection between the external resistor and the cathode and anode was discontinued so that the system became a separate constructed wetland system. However, it still used the water inlet and water outlet operation mode. A total of four different COD concentrations (230, 460, 690, and 1000 mg/L) were used, the total hydraulic retention time was 5 days, and samples were taken every 24 h. After filtration, the COD concentration in the top outlet solution was measured and the COD removal effects of CW and CW-MFC systems were compared.

Figure 5 shows a comparison of the COD removal effects of the CW and CW-MFC systems. It can be seen that both systems have good COD removal effects. The COD removal effect of the CW-MFC system with either the garnet of magnesia matrix was better than that of the CW system. The COD removal rate of the CW and CW-MFC systems with the garnet matrix was lower than that of the magnesia-based systems. The reason for the overall high removal rate by the CW-MFC system compared to the CW system may be that the redox reaction in the MFC system consumes organic matter and converts it into electricity. When the system generates electricity, an electrochemical reaction takes place to remove pollutants by electrolysis. The stable electricity generation system promotes the growth and reproduction of microorganisms, which subsequently leads to an increase in pollutant degradation. These results also show that the MFC system has a positive effect on COD removal.

3.3 Power generation performance of the CW-MFC system

The system operation is divided into five stages. The two CW-MFCs based on magnesia or garnet were operated at the same time. The first stage was the establishment and trial operation of the experimental device. The cathode and anode were connected with an external 1000 Ω resistor. Simulated domestic sewage without phosphorus was introduced and the voltage was monitored. During the second stage, the two microbial fuel cell systems were operated together. The pollutant concentration was 1 mg/L total phosphorus and the COD concentration was 230 mg/L. The pollutant concentration during the third stage was 2 mg/L total phosphorus and 460 mg/L COD, the pollutants concentration during the fourth stage was 3 mg/L total phosphorus and 690 mg/L COD, and the pollutant concentration during the fifth stage was 5 mg/L total phosphorus and 1000 mg/L COD.

It can be seen from Fig. 6 that the highest output voltage and stable voltage of the garnet device was greater than the magnesia device. During the third stage, the total phosphorus concentration was 2mg/L and COD concentration was 460 mg/L, and both devices reached their maximum output voltage. The maximum stable power generation voltage of the garnet device was 500 mV, and the maximum stable power generation voltage of the magnesia device was 290 mV. Temperature, the concentration of dissolved oxygen at the cathode, and the COD load at the anode all affected the voltage level.

In order to test the power generation performance of the CW-MFCs, the best power generation stage for the magnesia and garnet systems, namely the third stage, was used to conduct current density and power density tests. After the systems were stable, a 10–5000 Ω external resistor between the anode and cathode was connected and the output voltage at both ends of the external resistor was measured to obtain the system polarization curve and power density curve.

It can be seen from Fig. 7 that when the open circuit voltage of the garnet (a) matrix was 0.75 mV and the internal resistance was 245 Ω, the maximum power density was 0.48 W/m^3, and the maximum current density was 2.1 A/m^3. The open circuit voltage of the magnesia (b) device was 0.53 mV, the internal resistance was 450 Ω, and the greatest power density was 0.33W/m^3. The results show that the open circuit voltage was determined by the internal resistance. The smaller the internal resistance, the greater the open circuit voltage value and the system power generation capacity.

3.4 Microbial community structure in wetlands

(1) Community structure characteristics of soil microorganisms in wetland sediments

At the phylum level, there were nine dominant microbial groups with an average relative abundance of > 0.1% and their relative abundance accounted for 85.8–86.6% of the total microbial community. The D10 layer mainly consisted of *Proteobacteria* (38.5%), *Cyanobacteria* (25.1%), *Bacteroidetes* (12.4%), and *Gemmatimonadetes* (3.7%), which accounted for 79% of the total microbial community. Five phyla changed significantly between the D30 layer and the D10 layer. These were *Proteobacteria* (32.2%), *Cyanobacteria* (21.2%), *Bacteroidetes* (7.3%), *Gemmatimonadetes* (8.7%), and *Acidobacteria* (5.7%). There were three phyla whose relative decreased in the D30 layer compared to the D10 layer (Fig. 8a): *Proteobacteria*, *Bacteroidetes*, and *Cyanobacteria*, but their change in relative abundances were positive at 6.30%, 5.10%, and 3.90%, respectively (Fig. 8b). The phyla whose relative abundances increased the most between the D10 and D30 layers were *Gemmatimonadetes*, *Firmicutes*, *Acidobacteria*, *Actinobacteria*, and *Nitrospirae*, but their change in relative abundance was − 5.00%, − 2.20%, − 4.40%, − 0.60%, and − 2.60%, respectively (Fig. 8b).

At the genus level, the > 0.1% relative abundance groups were classified as the dominant genera. The main dominant groups in the D10 layer were *Nitrospira* (2.8%), *Rhodobacter* (2.4%), *Sphingomonas* (7.2%), *Tabrizicola* (2.1%), *Nevskia* (1.1%), and *Devosia* (1.3%) (Fig. 9a). The main dominant groups in the D30 layer were *Nitrospira* (3.4%), *Rhodobacter* (1.2%), *Sphingomonas* (2.1%), *Haliangium* (1.7%), and *H16* (1.6%). *Nitrospira*, *Haliangium*, *H16*, *Opitutus*, and *Pseudomonas* (Fig. 9a), whose relative abundances increased by 0.60%, 0.99%, 0.64%, 6.38%, and 0.36%, respectively. The genera that showed the most obvious decreases in relative abundance were *Rhodobacter*, *Sphingomonas*, *Tabrizicola*, *Devosia*, and *Porphyrobacter*, which decreased by 1.20%, 5.10%, 1.21%, 0.46%, and 0.34%, respectively. (Fig. 9b).

As shown in Fig. 10, at the wetland electrode, there were nine dominant microbial groups with an average relative abundance of > 1% at the phylum level, and their relative abundance accounted for 75.0–77.9% of the total microbial community. At the electrodes, *Proteobacteria* (34.5%), *Cyanobacteria* (19.0%), *Bacteroidetes* (6.3%) and *Gemmatimonadetes* (5.7%) were the main groups present, and these groups accounted for 77.1% of the total microbial community.

At the wetland electrode, the groups with an average relative abundance of > 0.1% at the genus level were classified as the dominant genera. The dominant genera groups were *Nitrospira* (2.4%), *Rhodobacter* (1.50%), *Sphingomonas* (4.30%), *Tabrizicola* (1.25%), *Nevskia* (0.76%), and *Devosia* (1.13%).

An analysis and comparison of the microbial community structure at the phylum level and genus level in the D10 and D30 layers of the wetland sediment soil showed that *Proteobacteria* and *Bacteroidetes* became more dominant at the phylum level, and the dominant microorganisms accounted for 85.8–86.6% of the total microbial community. At the genus level, *Haliangium* and *Opitutus* accounted for 23.29–24.23% of the microbial community. When the amount of microorganisms in the sediment and the electrode were compared, the microbial population at the electrode was significantly lower than that in

the sediment, but the migration of microorganisms became the main reason for the increase in electricity generation efficiency. The results suggest that when the CW-MFC system was operational, the significant changes in these microorganisms affected the removal of organic matter in the system and the electrical generation efficiency.

3.5 Analysis of the phosphorus removal mechanism used by the two matrices

3.5.1 Scanning electron microscopy

Figures 12 and 14 show the original state of the magnesia and garnet surface structure, respectively. It can be seen that magnesia and garnet surface are relatively rough, and the magnesia surface has a typical crystal structure. There are a large number of small protrusions on the magnesia matrix surface, whereas the garnet surface has a large number of lamellar structures and fine pores, which make it more suitable for microbial adhesion. Figures 13 and 15 are electron microscopic images of the magnesia and garnet surfaces after sewage water treatment. It can be seen that dense biofilms have formed on the surfaces of both the magnesia and garnet matrices and that the biofilm layer on the garnet matrix surface is greater than that on the magnesia surface. This may be because the surface of the garnet matrix has more and finer pores that induce the formation of biofilm on the surface of matrix. This biofilm plays an important role in the treatment of pollutants and enhances the effect of phosphorus degradation.

3.5.2 XRD detection and analysis

An XRD analysis was used to further explore the dephosphorization mechanism used by the matrices, and the object images of the matrices before and after the reaction were analyzed. The XRD images are shown in Figs. 16 and 17.

Figure 16 shows that the main component of magnesia is MgO. After dephosphorization, $Mg_3(PO_4)_2$ appears at 27.5°, and $MgHPO_4$ appears at 55.3°. Magnesium oxide dissolves in water and releases Mg^{2+} and OH^- and the ions diffuse outward. The phosphate ions in the water are released to the surface of the substrate to react with magnesium ions on the surface of the magnesia to form a magnesium phosphate precipitate. The large numbers of hydrogen phosphate ions in the alkaline water react with magnesium ions to form a magnesium hydrogen phosphate precipitate. Therefore, it is probable that the magnesia phosphorus removal mechanisms are mainly adsorption and reactions between ions.

The composition of the garnet matrix is relatively complex because it contains FeO, MgO, and other components. The removal of phosphorus by the garnet matrix mainly depends on a complex adsorption process and an ion exchange reaction that is similar to magnesia. It can be seen that after the reaction, $Mg_4(PO_4)_2OH$ appears at 33.5°, $AlPO_4(H_2O)_{1.5}$ appears at 66.7°, and $CaPO_4$ appears at 31.6°. Magnesium, aluminum, and calcium ions are all present in garnet. The main components diffuse into the water from the surface of the substrate and easily react with the phosphate and hydrogen phosphate

ions that are free in the sewage to form a precipitate. This precipitate then becomes attached to the surface of the substrate.

3.5.3 Isothermal adsorption

The isothermal adsorption curve can explain the relationship between the absorbate equilibrium concentration and equilibrium adsorption in solution at a certain temperature. In this experiment, two commonly used isothermal adsorption models were selected for investigation, which were the Langmuir and Freundlich isothermal adsorption models. The complex adsorption process means that it is not presently known what the exact adsorption mechanism is. This experiment assumed that the adsorbent surface was uniform, the adsorption process took place in the monolayer, absorption takes place uniformly across the matrix surface, and the maximum adsorption amount is reached after the surface adsorbent is saturated.

Tables 5 and 6 show the linear fitting regression equation parameters for the three substrates and the two models:

Table 5
Langmuir isotherm adsorption curve results

Substrate	KL	qm	R^2	1/KLqm	Linear regression equation
cordierite	0.018	0.29	0.9999	182.6	1/qe = 182.6/Ce + 3.448
magnesia	0.16	2.328	0.9891	0.0713	1/qe = 0.0713/Ce + 0.429
garnet	0.15	1.675	0.9371	3.98	1/qe = 3.98/Ce + 0.597

Table 6
Freundlich isotherm adsorption curve results

Substrate	KF	1/n	R^2	Linear regression equation
cordierite	0.006	0.96	0.9996	Lnqe = 0.96lnCe – 2.813
magnesia	1.928	0.48	0.9662	Lnqe = 0.48lnCe + 0.66
garnet	1.294	0.68	0.9114	Lnqe = 0.68lnCe + 0.258

As shown in the Figs. 18–20 and Tables 5 and 6, cordierite, magnesia, and garnet all have good correlations when the *Langmuir* isothermal adsorption model is applied, and the corresponding coefficients R^2 are 0.9999, 0.9891, and 0.9371, respectively. The results suggest that phosphorus is absorbed by the monolayer on the cordierite, magnesia, and garnet surfaces. The maximum theoretical

adsorption capacities were 0.29, 2.328, and 1.675 mg/g, respectively. The KL values were 0.018, 0.16, and 0.15 on average, and in the 10–70 mg/L concentration range, the KL values for magnesia and garnet were much higher than for cordierite. In general, the adsorption capacity order for phosphorus was magnesia > garnet > cordierite. Therefore, the magnesia absorption capacity represents the theoretical maximum adsorption capacity.

In the *Freundlich* isothermal adsorption model, cordierite, magnesia, and garnet also show good linear relationships, and the corresponding R^2 coefficients were 0.9996, 0.9662, and 0.9114, respectively. The results suggest that the cordierite, magnesia, and garnet adsorption process is inter-molecular chemisorption. The KF values were 0.006, 1.928, and 1.294 respectively, and the descending order for absorption was magnesia > garnet > cordierite. The higher the KF value, the better the adsorption performance. The magnesia and garnet adsorption performances were similar, and much higher than that of cordierite. At the same time, the smaller the value of 1/n, the easier the adsorption reaction is.

Cordierite, magnesia, and garnet conform to both the Langmuir and Freundlich equations. This suggests that the phosphorus absorption mechanisms for the three substrates are mono-molecular physical adsorption and multi-molecular chemical adsorption at the same time. Magnesia showed the best phosphorus adsorption capacity and cordierite showed the worst adsorption capacity in this experiment.

4 Conclusion

The purpose of this study was to provide a reference for the selection of phosphorus removal substrates when constructing a wetland coupled microbial fuel cell system. Overall, the system has a good phosphorus removal effect. The garnet substrate had the highest total phosphorus removal rate at 92.4% and the magnesia substrate removal rate was 80.3%. The removal effect of the garnet substrate was better than that of magnesia, but the higher the concentration of influent pollutants, the worse the treatment effect. The biofilm layer on the surface of the garnet was greater than on the magnesia surface. The formation of biofilm on the surface of a substrate plays an important role in the treatment of pollutants and enhances phosphorus degradation. The reason the garnet biofilm could absorb more phosphorus was that the garnet surface had more and finer pores. Furthermore, the removal of phosphorus by the garnet matrix is mainly caused by the diffusion of the garnet components from the surface of the substrate into the water solution where they can easily react with free phosphate and hydrogen phosphate ions in the sewage forming precipitates that attach to the surface of the substrate. The magnesia dephosphorization mechanisms are mainly adsorption and reactions between and ions. The phosphorus adsorption capacity of magnesia is higher than that of garnet, which may be due to the physical adsorption by the monolayer combined with multi-layer chemical adsorption. The magnesia showed the best phosphorus adsorption capacity, but there was actually little difference between magnesia and garnet. The CW-MFC system shows good power generation capacity. The highest output voltage and the stable voltage of the garnet substrate were higher than those of the magnesium substrate. The devices with the two different substrates reached their maximum output voltage when the COD and total phosphorus concentrations were both 460 mg/L. The maximum stable voltage of the

garnet device was 500 mV and the maximum stable generating voltage of the magnesia device was 290 mV. The microorganisms in the wetland sediment soils and at the electrodes substantially changed, indicating that the microorganisms positively respond to the removal of organic matter and power generation.

In this study, the garnet and magnesia had very good phosphorus removal rates and could efficiently generate electricity. Future studies should investigate phosphorus removal and electricity generation by other substrates. This technology combines the advantages of constructed wetlands and microbial fuel cells, and uses both sewage treatment and electricity output to optimize the coupling system for phosphorus removal. Therefore, when studying CW-MFCs, the selection of electrode materials, substrate, and system structure need to be taken into account when attempting to improve phosphorus removal and the power generation capacity of the system.

5 Declarations

Ethical Approval

The study is not applicable for that section.

Consent to Participate

Informed consent was obtained from all individual participants included in the study.

Consent to Publish

All authors have agreed to submit the study.

Authors Contributions

Shuang Yu: Data curation, Concept. Peng Dou and Yue Yin: Software, Investigate.Peijing Wang and Hao Wang: Supervision. Jinlong Han: Software, Investigate. Duo Xu: Writing reports.

Funding

National Science Foundation for Young Scientists of China (No.51709279).

Competing Interests

The authors have no relevant financial or non-financial interests to disclose.

Availability of data and materials

The data and materials used in this study came from the laboratory.

6 References

1. Abazarian E, Gheshlaghi R, Mahdavi M A (2020) Impact of light/dark cycle on electrical and electrochemical characteristics of algal cathode sediment microbial fuel cells. J Power Sources. 475:228686. http://dx.doi.org/10.1016/j.jpowsour.2020.228686.
2. Ahmadpour T, Aber S, Hosseini M G (2020) Improved dye degradation and simultaneous electricity generation in a photoelectrocatalytic microbial fuel cell equipped with AgBr/CuO hybrid photocathode. J Power Sources. 474:228589. http://dx.doi.org/10.1016/j.jpowsour.2020.228589.
3. Colares G S, 'Osbel N D, Barbosa C V, Lutterbeck C, Machado N L (2020). Floating treatment wetlands integrated with microbial fuel cell for the treatment of urban wastewaters and bioenergy generation. Sci Total Environ. 142474. http://dx.doi.org/10.1016/j.scitotenv.2020.142474.
4. Deng S, Xie B, Kong Q, Peng S, Li D (2020) An oxic/anoxic-integrated and Fe/C micro-electrolysis-mediated vertical constructed wetland for decentralized low-carbon greywater treatment. Bioresource Technol. 315. http://dx.doi.org/10.1016/j.biortech.2020.123802.
5. Fhl A , Hong Q , Fvk A , Wi B, Vd C, Jd D, Dplr A, Swhvh A (2020) Water treatment and re-use at temporary events using a mobile constructed wetland and drinking water production system. Sci Totla Environ. 2020737. http://dx.doi.org/10.1016/j.scitotenv.2020.139630.
6. Ge X, Cao X, Song X, Wang Y, Tesfahunegn A A (2019) Bioenergy generation and simultaneous nitrate and phosphorus removal in a pyrite-based constructed wetland-microbial fuel cell. Bioresource Technol. 296:122350. http://dx.doi.org/10.1016/j.biortech.2019.122350.
7. González T, Puigagut J, Vidal G (2020) Organic matter removal and nitrogen transformation by a constructed wetland-microbial fuel cell system with simultaneous bioelectricity generation. Sci Total Environ. 753:142075. http://dx.doi.org/10.1016/j.scitotenv.2020.142075.
8. Gupta S, Srivastava P, Patil S A, Kumar A (2020) A comprehensive review on emerging constructed wetland coupled microbial fuel cell technology: Potential applications and challenges. Bioresource Technol. 124376. http://dx.doi.org/10.1016/j.biortech.2020.124376.
9. Hai T, Min B (2020) Leachate treatment and electricity generation using an algae-cathode microbial fuel cell with continuous flow through the chambers in series. Sci Total Environ. 723:138054. http://dx.doi.org/10.1016/j.scitotenv.2020.138054.
10. Lei X, Zhao Y, Wang X, Yu W (2018) Applying multiple bio-cathodes in constructed wetland-microbial fuel cell for promoting energy production and bioelectrical derived nitrification-denitrification process. Chem Eng J. 344:105-113. http://dx.doi.org/10.1016/j.cej.2018.03.065.
11. Liang Y, Wei D, Hu J, Zhang J, Liu Z, Li A, Li R (2020) Glyphosate and nutrients removal from simulated agricultural runoff in a pilot pyrrhotite constructed wetland. Water Res. 168(Jan.1):115154.1-115154.7. http://dx.doi.org/10.1016/j.watres.2019.115154.
12. Li B, Yang Y, Chen J, Zhen W, Yong L, Xie S (2018) Nitrifying activity and ammonia-oxidizing microorganisms in a constructed wetland treating polluted surface water. Sci Totla Environ. s 628–629(JUL.1):310-318. http://dx.doi.org/10.1016/j.scitotenv.2018.02.041.
13. Lim S S, Fontmorin J M, Pham T H, Milner E, Yu E H (2021) Zinc removal and recovery from industrial wastewater with a microbial fuel cell: Experimental investigation and theoretical prediction.

Sci Total Environ. 145934. http://dx.doi.org/10.1016/j.scitotenv.2021.145934.

14. Liu R, Zheng X Y, Li M, Han L M, Fang X (2019) A three chamber bioelectrochemical system appropriate for in-situ remediation of nitrate-contaminated groundwater and its reaction mechanisms. Water Res. 04:047. http://dx.doi.org/10.1016/j.watres.2019.04.047.
15. Li X, Song H, Xiang W, Wu L (2012) Electricity generation during wastewater treatment by a microbial fuel cell coupled with constructed wetland. J of Southeast University (English Edition). 28(2):175-178. http://dx.doi.org/10.3969/j.issn.1003-7985.2012.02.008.
16. Mander L, Tournebize J, Espenberg M, Chaumont C, Soosaar K (2021) High denitrification potential but low nitrous oxide emission in a constructed wetland treating nitrate-polluted agricultural run-off. Sci Totla Environ. 779(19):146614. http://dx.doi.org/10.1016/j.scitotenv.2021.146614.
17. Ma Y, Dai W, Zheng P, Zheng X, Zhao M (2020) Iron scraps enhance simultaneous nitrogen and phosphorus removal in subsurface flow constructed wetlands. Journal Hazard Mater. 395:122612. http://dx.doi.org/10.1016/j.jhazmat.2020.122612.
18. Nguyen T, Ngo H H, Guo W S, Nguyen T H H, Pham T T (2020) White hard clam (Meretrix lyrata) shells media to improve phosphorus removal in lab-scale horizontal sub-surface flow constructed wetlands: Performance, removal pathways, and lifespan. Bioresource Technol. 312:123602. http://dx.doi.org/10.1016/j.biortech.2020.123602.
19. Niu Y, Liu X, Chang G, Guo Q (2020) Treatment of isopropanol wastewater in an anaerobic fluidized bed microbial fuel cell filled with macroporous adsorptive resin as multifunctional biocarrier. Sci Total Environ. 719(Jun.1):137495.1-137495.11. http://dx.doi.org/10.1016/j.scitotenv.2020.137495.
20. Oon Y L, Ong S A, Ho L N, Wong Y S, Nordin N (2018) Up-flow constructed wetland-microbial fuel cell for azo dye, saline and nitrate remediation and bioelectricity generation: from waste to energy approach. Bioresource Technol. 266. http://dx.doi.org/10.1016/j.biortech.2018.06.035.
21. Overbeek C C , Harpenslager S F , Zuidam J ,Loon E, Geest H (2020) Drivers of Vegetation Development, Biomass Production and the Initiation of Peat Formation in a Newly Constructed Wetland. Ecosystems. 23(1):1-18. http://dx.doi.org/10.1007/s10021-019-00454-x.
22. Patel D, Bapodra S L, Madamwar D, Desai C(2021) Electroactive bacterial community augmentation enhances the performance of a pilot scale constructed wetland microbial fuel cell for treatment of textile dye wastewater. Bioresource Technol. 125088. http://dx.doi.org/10.1016/j.biortech.2021.125088.
23. Pelissari C, Avila C, Trein C M, Garcia J, Armas R D D, Sezerino P H (2017) Nitrogen transforming bacteria within a full-scale partially saturated vertical subsurface flow constructed wetland treating urban wastewater. Sci Total Environ. 574(JAN.1):390-399. http://dx.doi.org/10.1016/j.scitotenv.2016.08.207.
24. Rodrigo M A, Valentín A, Claros J , Moreno L, Segura M, Lassalle M, Vera P (2018) Assessing the effect of emergent vegetation in a surface-flow constructed wetland on eutrophication reversion and biodiversity enhancement. Ecol Eng. 113:74-87. http://dx.doi.org/10.1016/j.ecoleng.2017.11.021.

25. Rout S, Parwaiz S, Nayak A K, Varanasi J L, Das D (2020) Improved bioelectricity generation of air-cathode microbial fuel cell using sodium hexahydroxostannate as cathode catalyst. J Power Sources. 450:227679. http://dx.doi.org/10.1016/j.jpowsour.2019.227679.
26. Schierano M C, Panigatti M C, Maine M A, Griffa C, Boglione R (2020) Horizontal subsurface flow constructed wetland for tertiary treatment of dairy wastewater: Removal efficiencies and plant uptake. J Environ Manage. 272:111094. http://dx.doi.org/10.1016/j.jenvman.2020.111094.
27. Tang X, Liu H, Nala R, Dai Y, Yang Y (2020) Irrigation using hybrid constructed wetland treated domestic sewage: Uptake of phthalic acid esters and antibiotics by Ipomoea aquatica Forssk. J Hazard Mater. 124025. http://dx.doi.org/10.1016/j.jhazmat.2020.124025.
28. Tunsiper B (2020) Nitrogen removal in an aerobic gravel filtration-sedimentation pond-constructed wetland-overland flow system treating polluted stream waters: Effects of operation parameters. Sci Total Environ. 746:140577. http://dx.doi.org/10.1016/j.scitotenv.2020.140577.
29. Uusheimo S, Huotari J, Tulonen T, Aalto S, Rissanen A, Arvola L (2018) High Nitrogen Removal in a Constructed Wetland Receiving Treated Wastewater in a Cold Climate. Environ Sci Technol. 52(22):13343-13350. http://dx.doi.org/10.1021/acs.est.8b03032.
30. Walaszek M, Bois P, Laurent J, Lenormand E, Wanko A (2018) Micropollutants removal and storage efficiencies in urban stormwater constructed wetland. Sci Totla Environ. 645:854. http://dx.doi.org/10.1016/j.scitotenv.2018.07.156.
31. Wang J L, Fu Z S, Qiao H X, Liu F X (2018) Assessment of eutrophication and water quality in the estuarine area of Lake Wuli, Lake Taihu, China.. Sci Total Environ. 137. http://dx.doi.org/10.1016/j.scitotenv.2018.09.137.
32. Wang Y, Wen Q, Chen Y, Zheng H, Wang S (2020) Enhanced performance of microbial fuel cell with polyaniline/sodium alginate/carbon brush hydrogel bioanode and removal of COD. Energy. 202:117780. http://dx.doi.org/10.1016/j.energy.2020.117780.
33. Wen H, Zhu H, Yan B, Shutes B, Yu X, Chen R, Chen X, Wang X (2021) Constructed wetlands integrated with microbial fuel cells for COD and nitrogen removal affected by plant and circuit operation mode. Environ Sci Pollut R. 28(3):3008-3018. http://dx.doi.org/10.1007/s11356-020-10632-3.
34. Wu Q, Jiao S, Ma M, Peng S (2020) Microbial fuel cell system: a promising technology for pollutant removal and environmental remediation. Environ Sci Pollut R. 27(7):6749-6764. http://dx.doi.org/10.1007/s11356-020-07745-0.
35. Xu F, Cao F Q, Kong Q, Zhou L L, Yuan Q, Zhu Y J, Wang Q, Du Y D, Wang Z D (2018) Electricity production and evolution of microbial community in the constructed wetland-microbial fuel cell. Chem Eng J. S1385894718301840. http://dx.doi.org/10.1016/10.1016/j.cej.2018.02.003.
36. Xu G, Zheng X, Lu Y, Liu G, Luo H, Li X, Zhang R, Jin S (2019) Development of microbial community within the cathodic biofilm of single-chamber air-cathode microbial fuel cell. Sci Total Environ. 665(MAY 15):641-648. http://dx.doi.org/10.1016/j.scitotenv.2019.02.175

37. Xu H, Song H L, Singh R P, Yang Y L, Yang X L (2021) Simultaneous reduction of antibiotics leakage and methane emission from constructed wetland by integrating microbial fuel cell. Bioresource Technol. 320:124285. http://dx.doi.org/10.1016/j.biortech.2020.124285.
38. Yan Z, He Y, Cai H, Nostrand J D, He Z, Zhou J, Krumholz L R, Jiang H L (2017) Interconnection of Key Microbial Functional Genes for Enhanced Benzo[a]pyrene Biodegradation in Sediments by Microbial Electrochemistry. Environ Sci Technol. 51(15):8519-8529. http://dx.doi.org/10.1021/acs.est.7b00209.
39. Yang X, Chen S (2020) Microorganisms in sediment microbial fuel cells: Ecological niche, microbial response, and environmental function. Sci Total Environ. 756(19):144145. http://dx.doi.org/10.1016/j.scitotenv.2020.144145.
40. Zhang S, Yang X L, Li H, Song H L, Wang R C, Dai Z Q (2017) Degradation of sulfamethoxazole in bioelectrochemical system with power supplied by constructed wetland-coupled microbial fuel cells. Bioresource Technol. 345. http://dx.doi.org/10.1016/j.biortech.2017.07.143.
41. Zhou S, Wang C, Liu C, Sun H, Xin L (2020) Nutrient removal, methane and nitrous oxide emissions in a hybrid constructed wetland treating anaerobic digestate. Sci Totla Environ. 733:138338. http://dx.doi.org/10.1016/j.scitotenv.2020.138338.

Figures

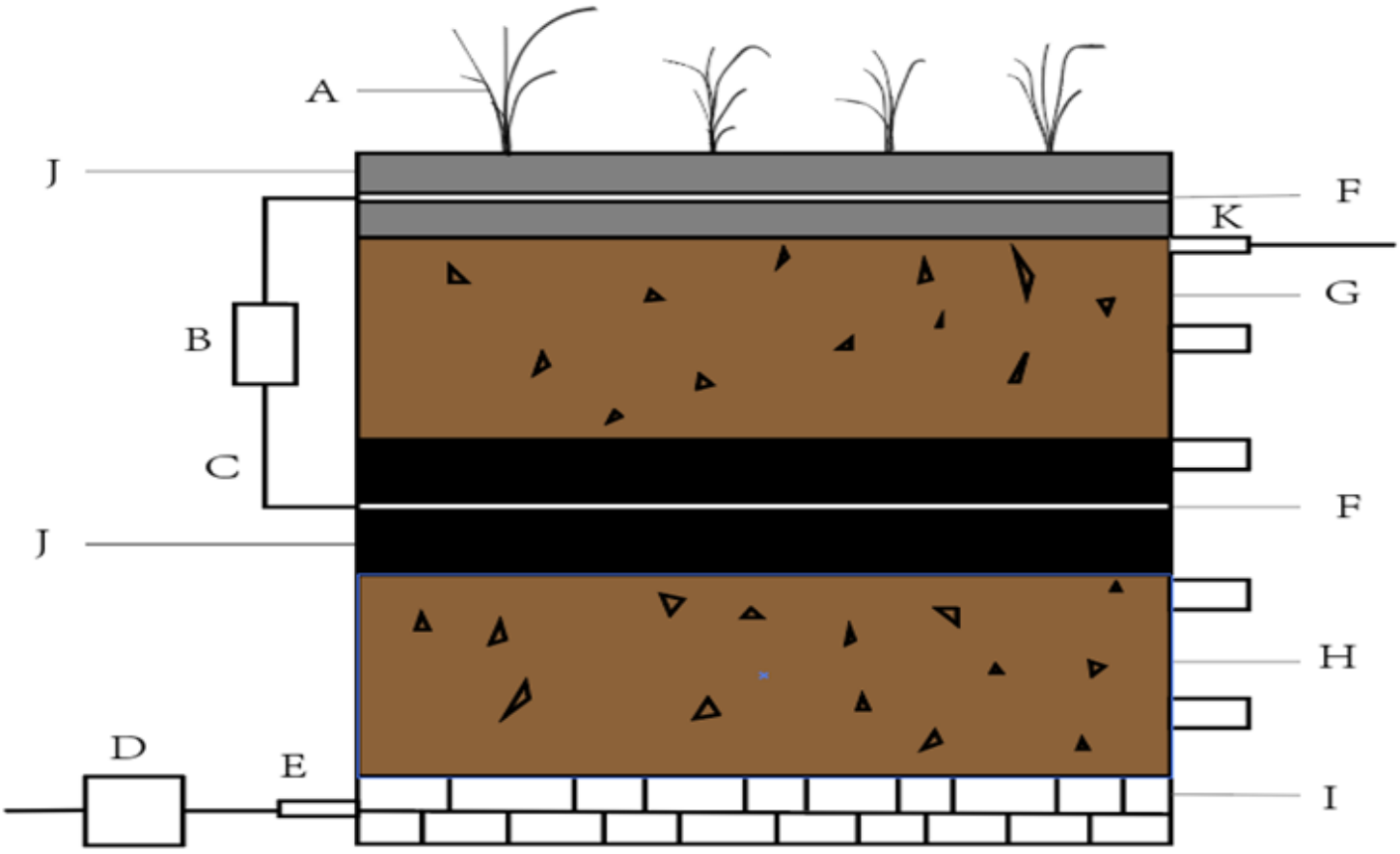

Figure 1

Diagram of the experimental device A- wetlandplant; B- resistance; C- copper wire; D- peristalticpump; E- waterinlet; F- stainlesssteelcloth; G- upper packing; H- lower packing; I- gravel; J- activatedcarbon; K- deliveryport.

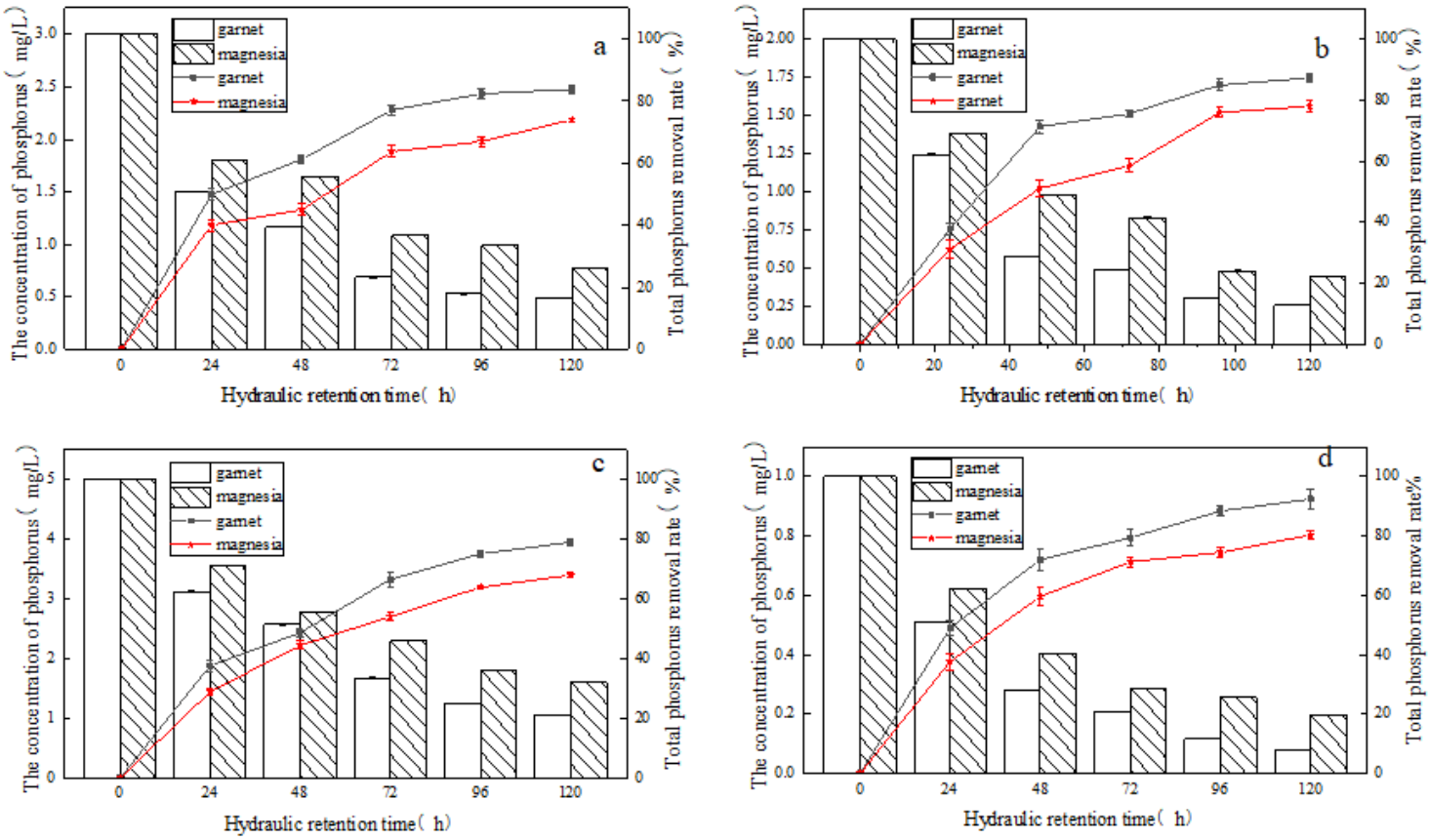

Figure 2

Total phosphorus concentrations and removal rates a: 1 mg/L, b: 2 mg/L, c: 3 mg/L, and d: 5 mg/L.

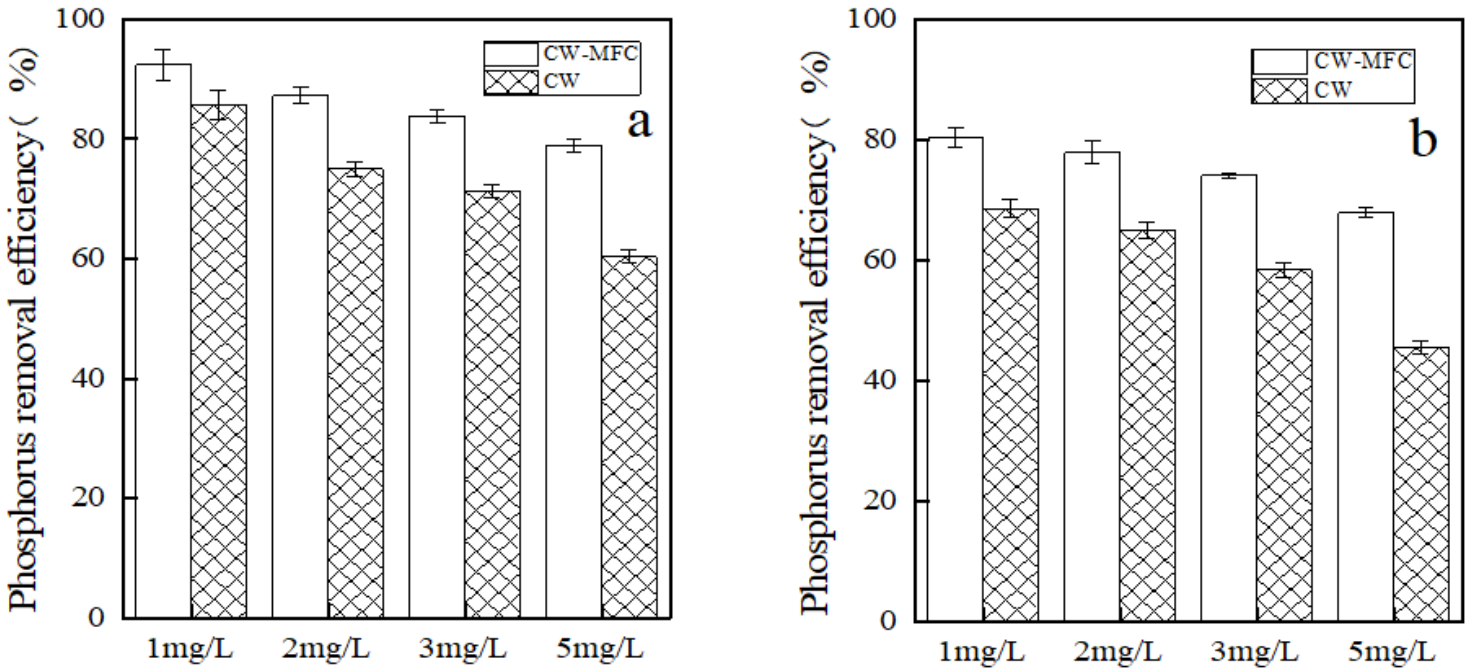

Figure 3

Phosphorus removal by the CW and CW-MFC systems (a) Constructed system based on garnet. (b) Constructed system based on magnesia.

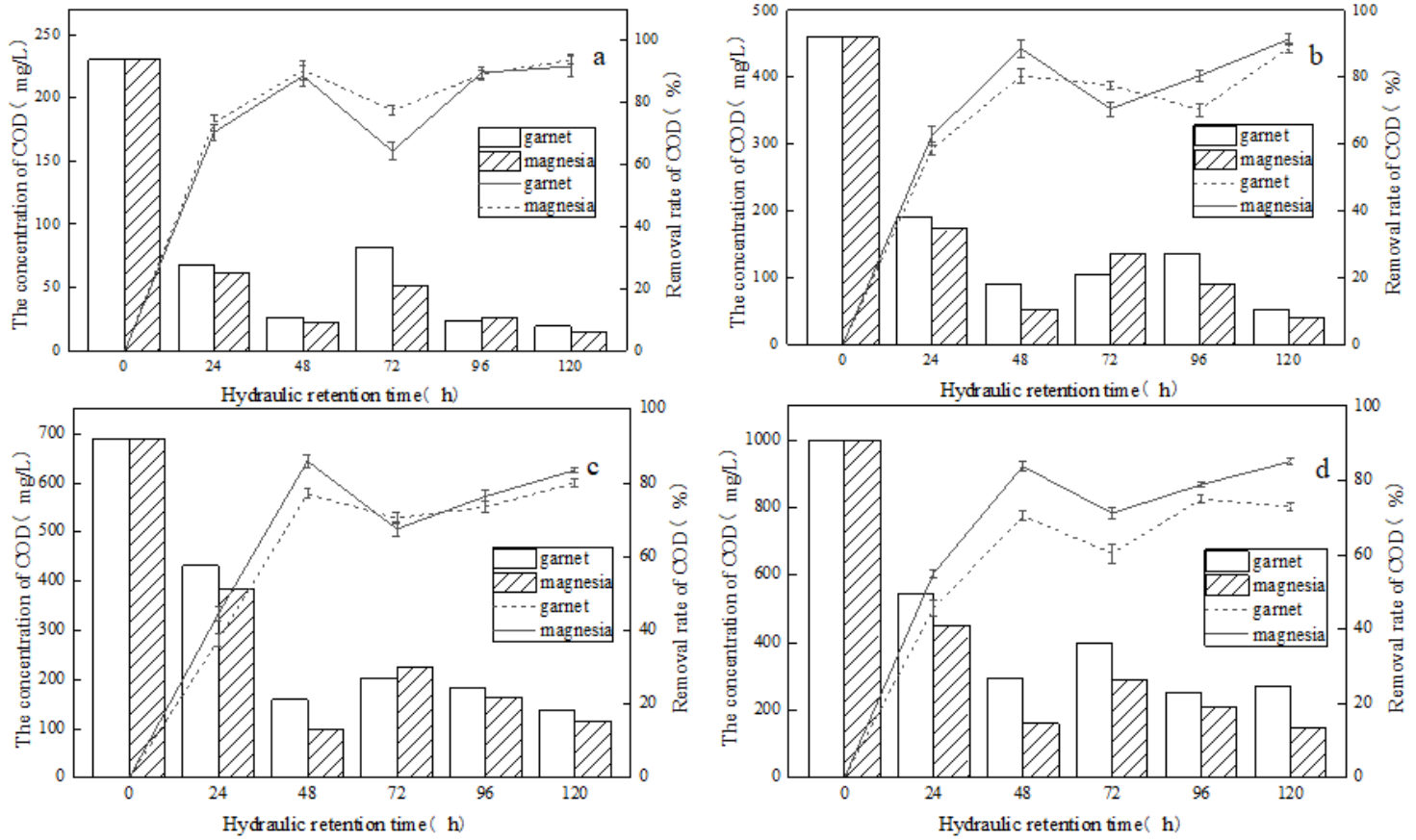

Figure 4

COD concentrations and removal rates (a) 230 mg/L influent COD concentration. (b) 460 mg/L influent COD concentration. (c) 690 mg/L influent COD concentration. (d) 1000 mg/L influent COD concentration.

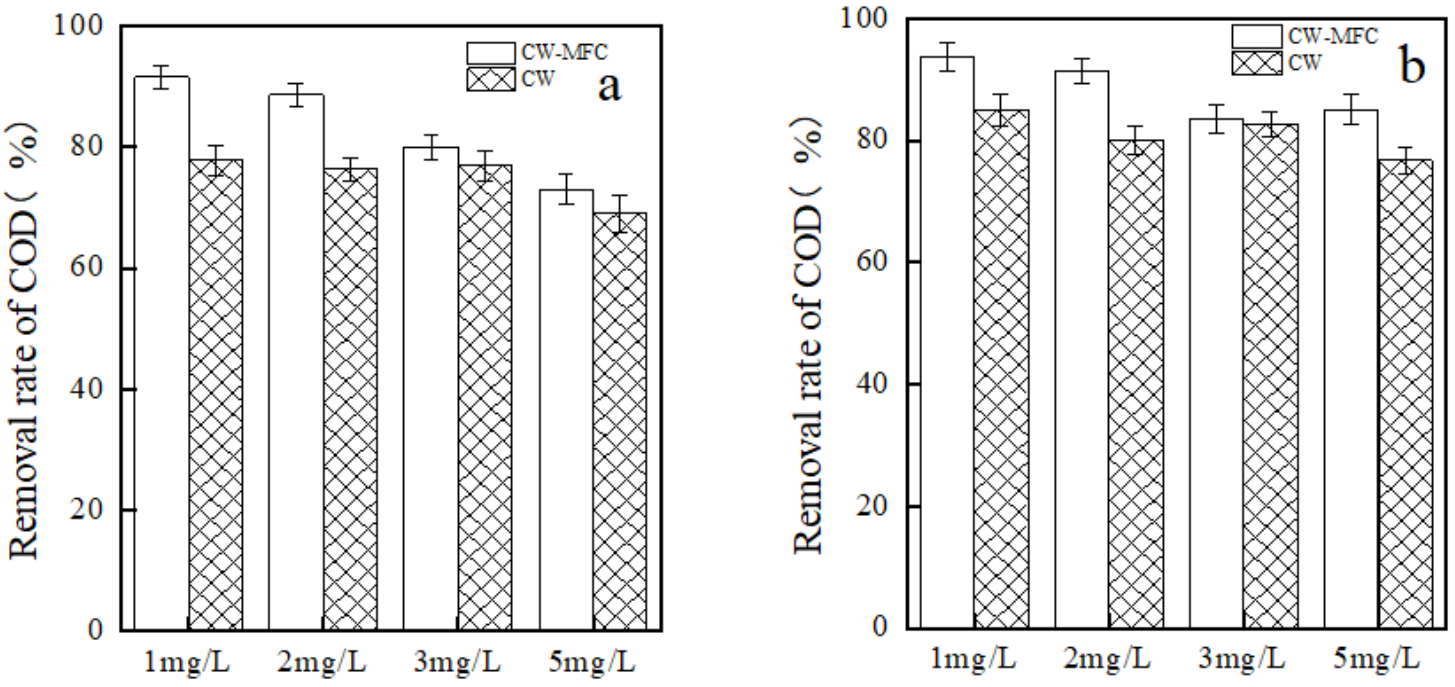

Figure 5

COD removal by theCW and CW-MFC systems (a) Constructed system based on garnet. (b) Constructed system based on magnesia

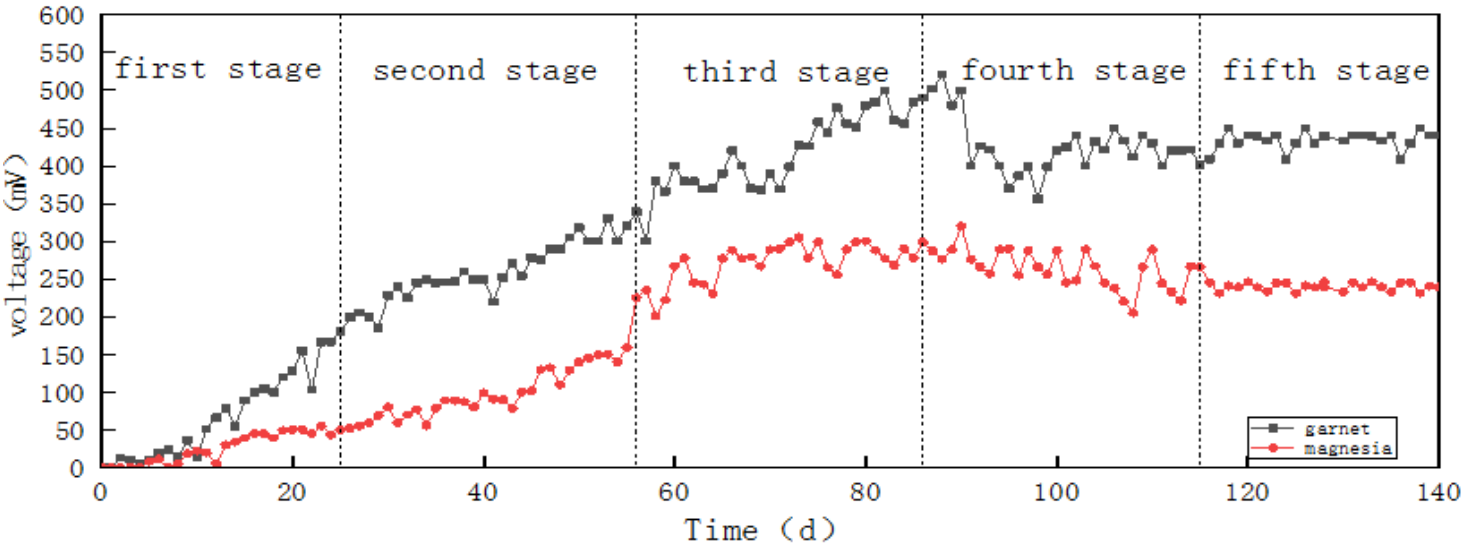

Figure 6

Daily voltage changes during the CW-MFC stages

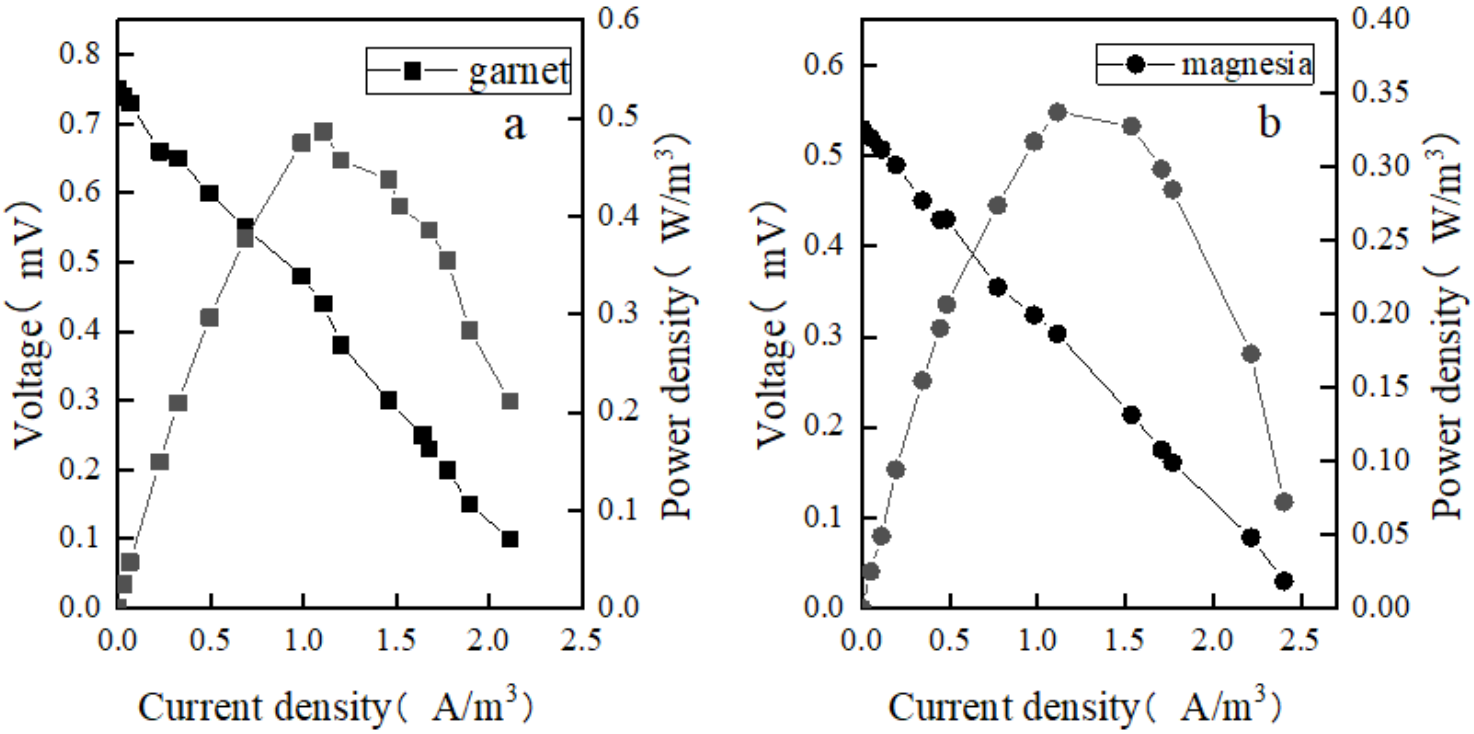

Figure 7

Polarization curve and power density curve (a) Garnet matrix. (b) Magnesia matrix

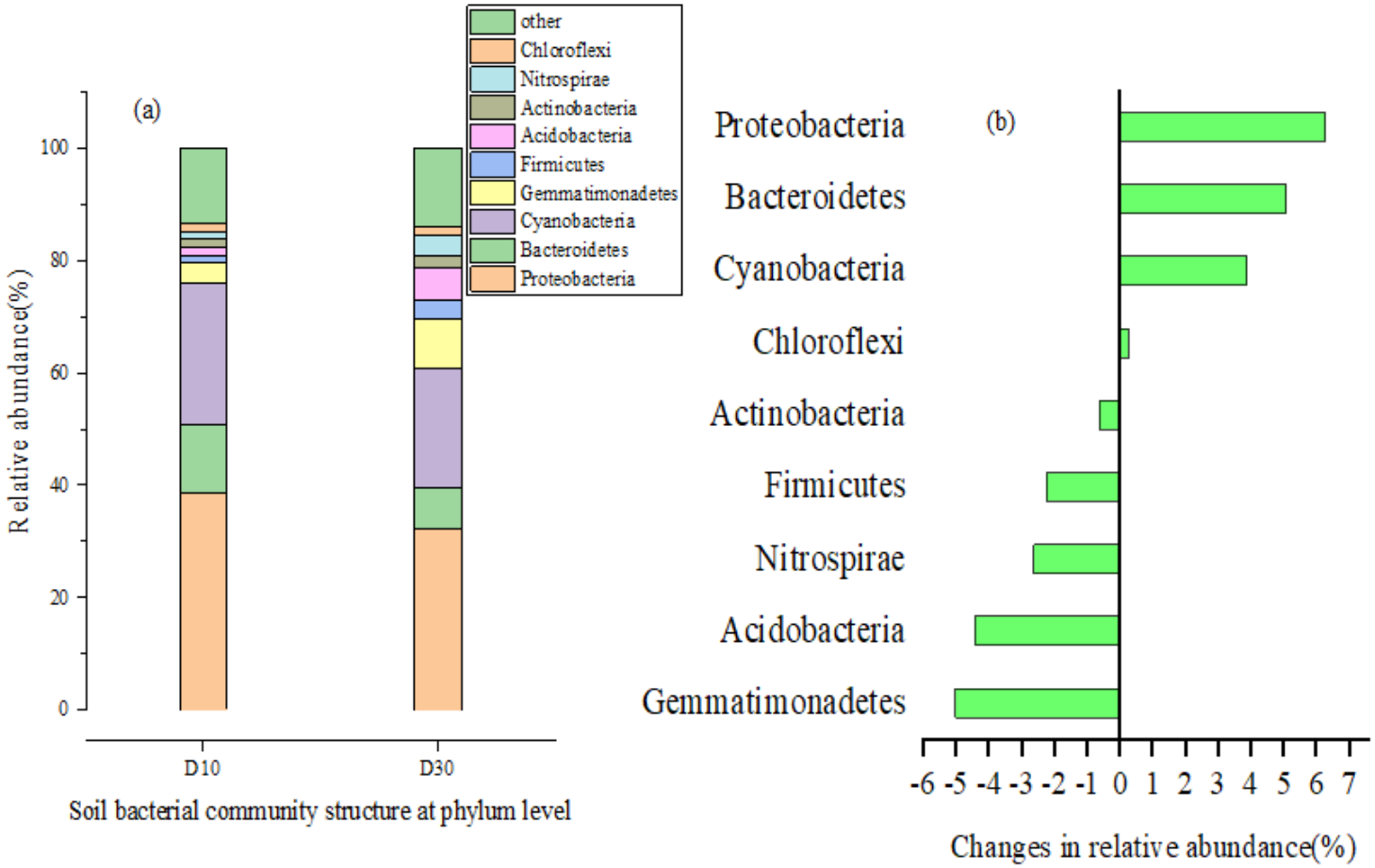

Figure 8

Soil microorganism changes in the wetland sediments at the phylum level

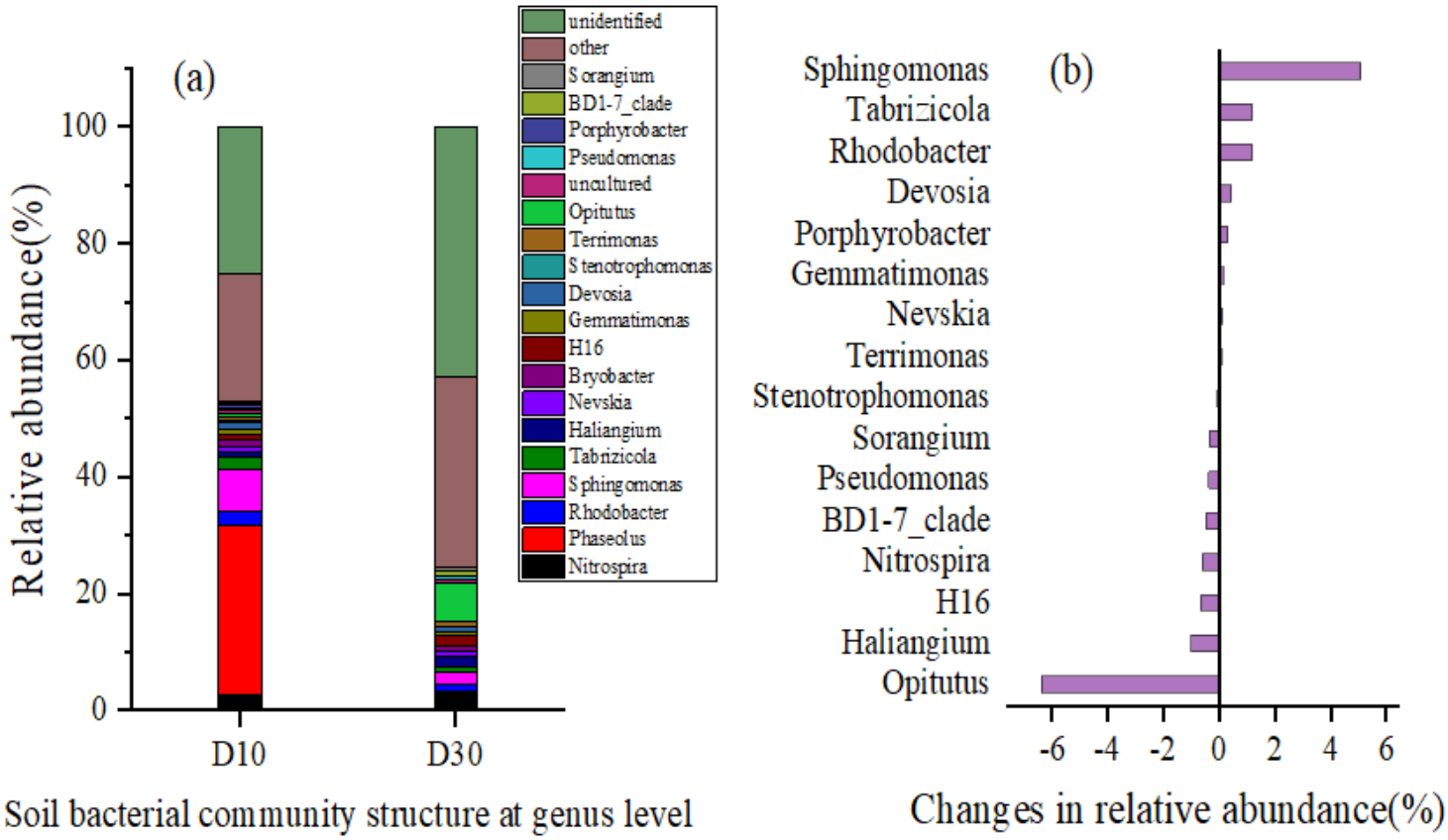

Figure 9

Soil microorganism changes in wetland sediments at the genus level

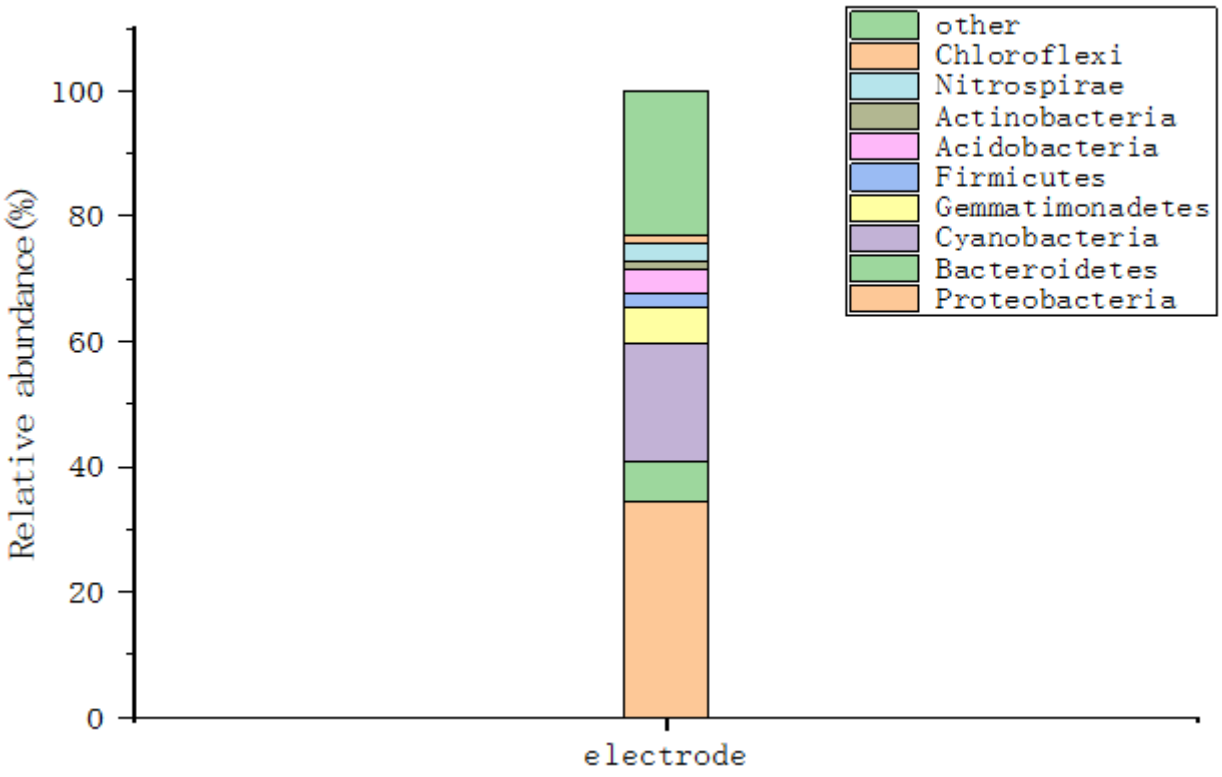

Figure 10

Microbial group level changes at the wetland electrode

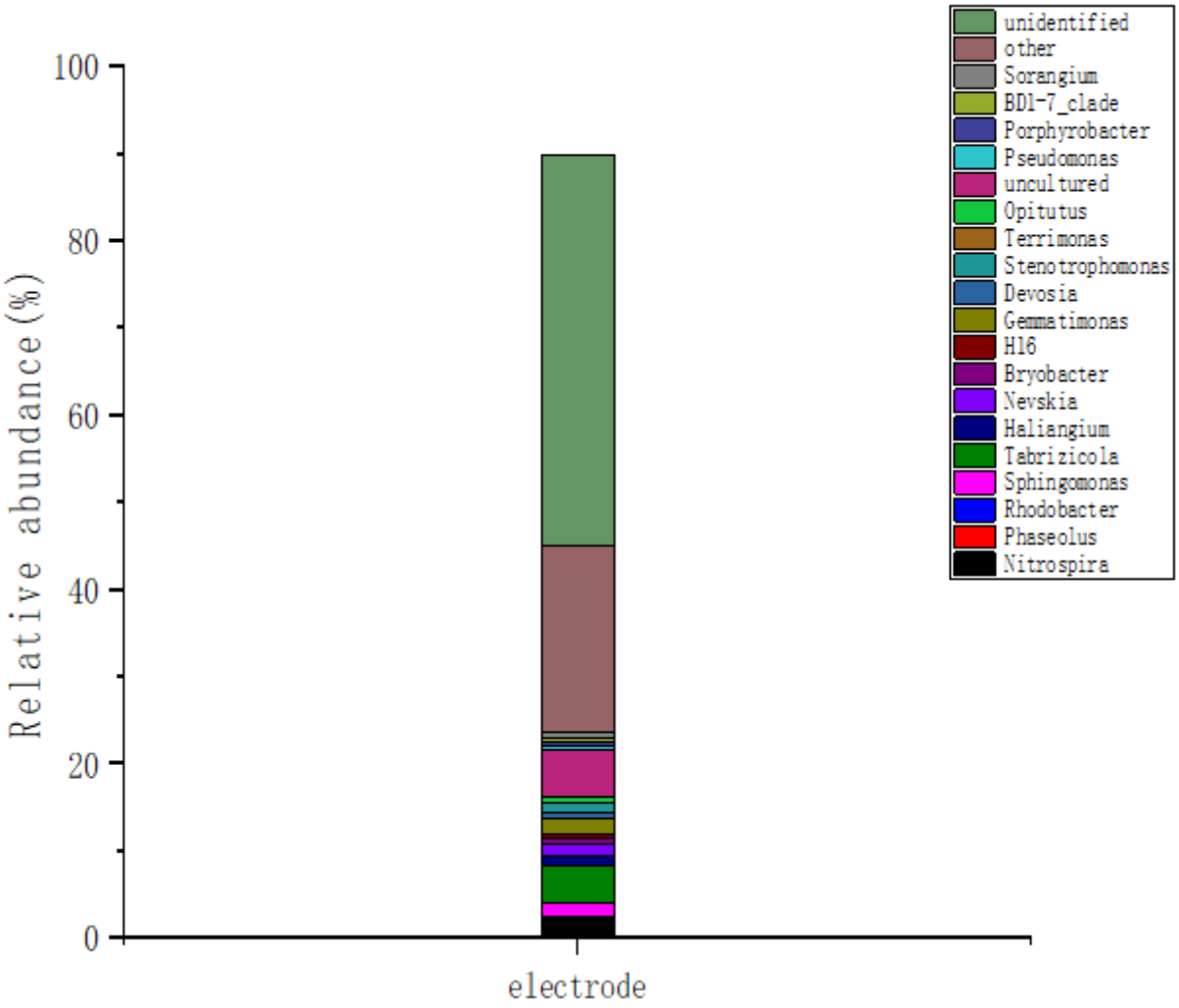

Figure 11

Changes in microbial genera at the wetland electrode

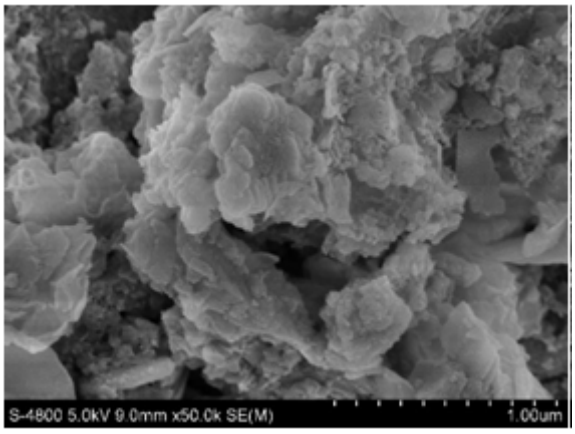

Figure 12

Magnesia matrix before treatment

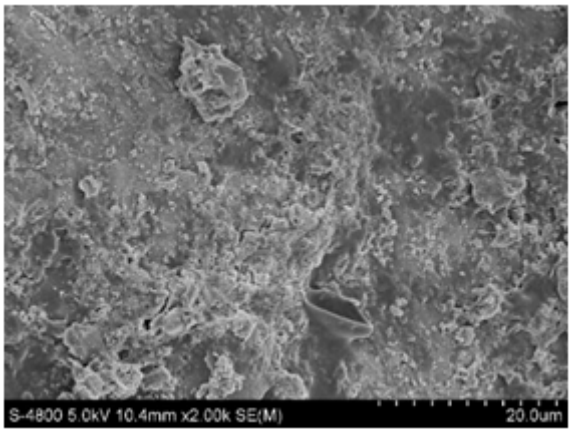

Figure 13

Magnesia matrix after treatment

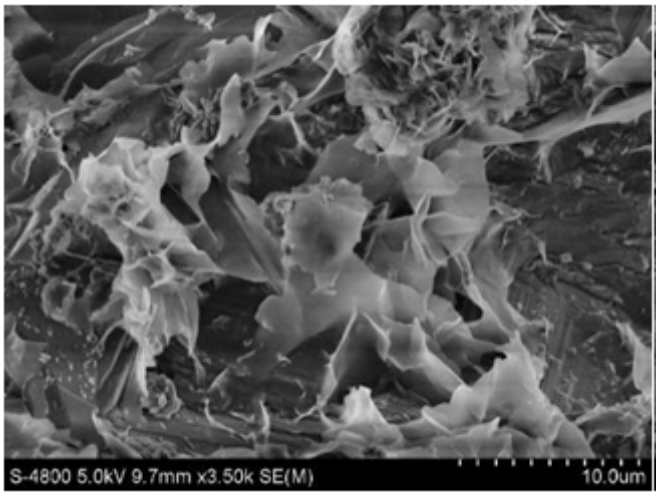

Figure 14

Garnet matrix before treatment

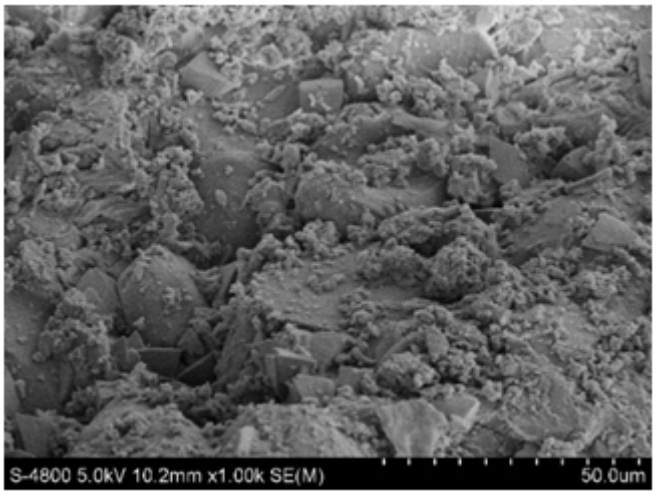

Figure 15

Garnet matrix after treatment

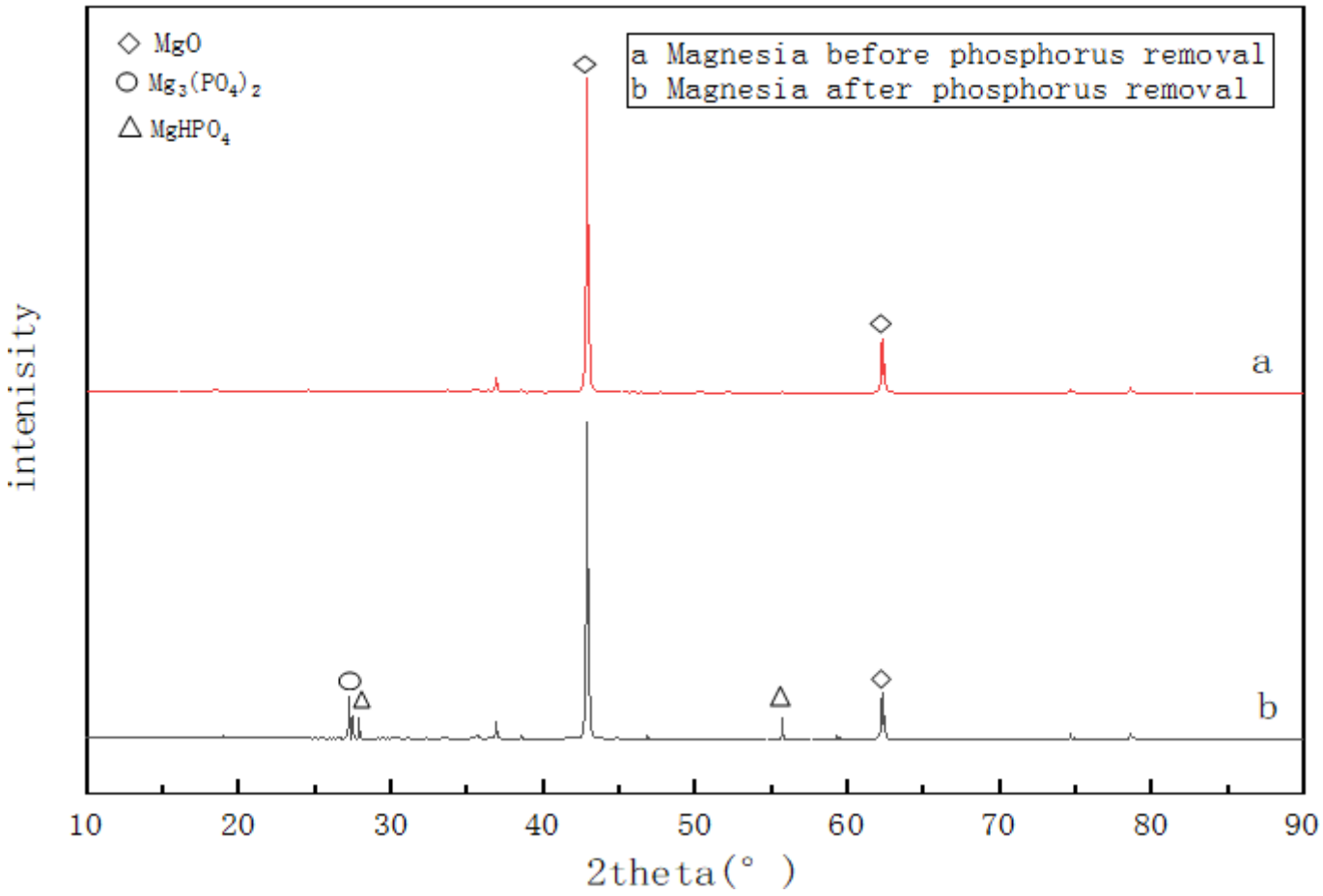

Figure 16

Magnesia XRD results

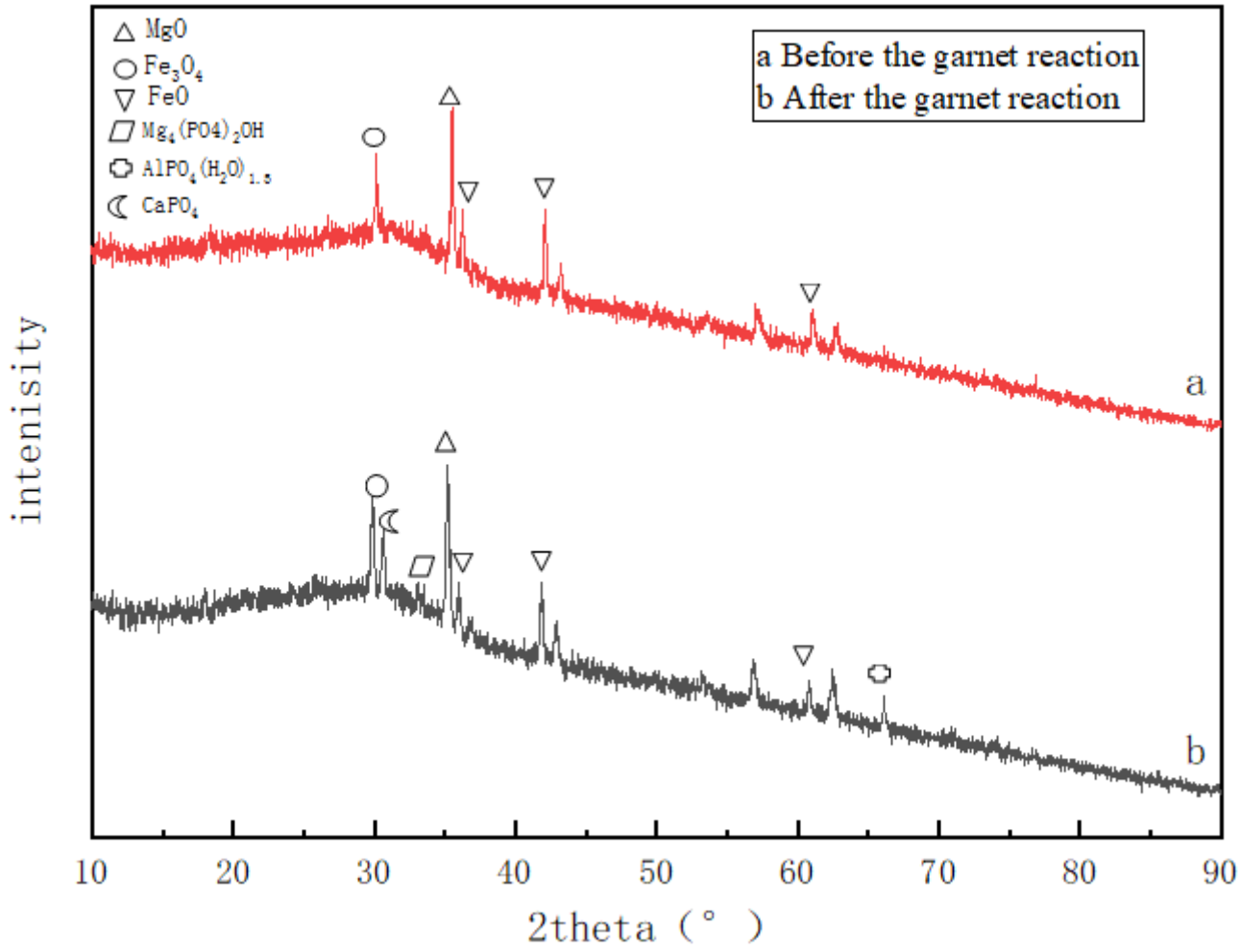

Figure 17

Garnet XRD results

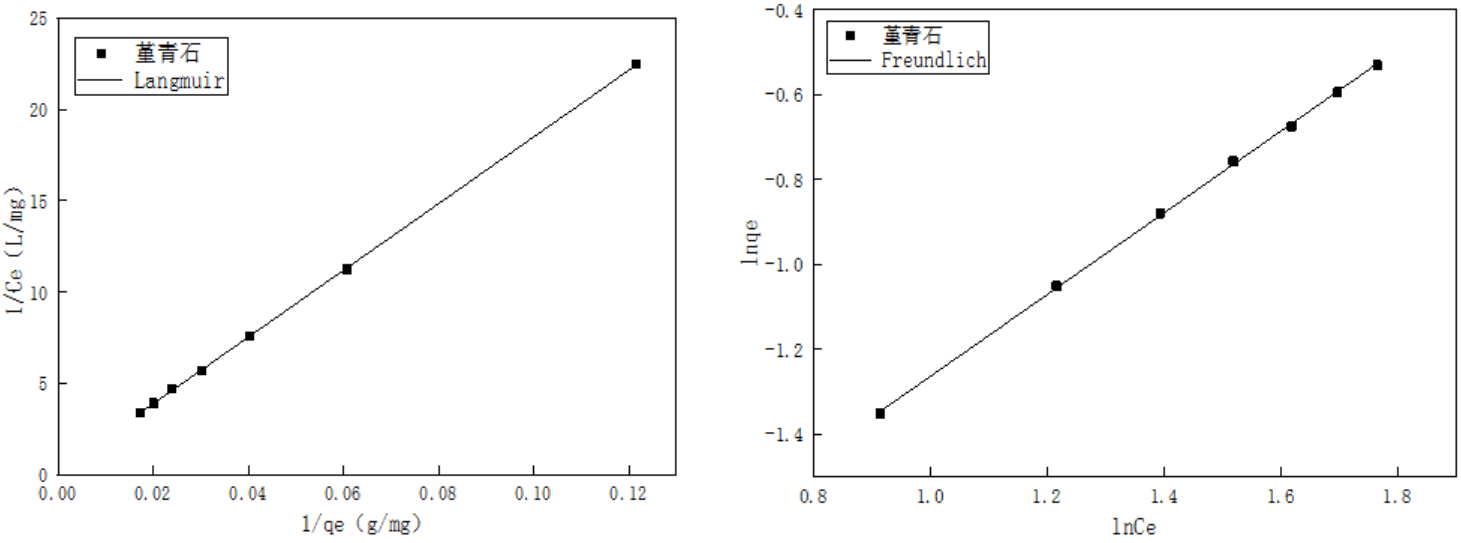

Figure 18

Isotherm adsorption by cordierite

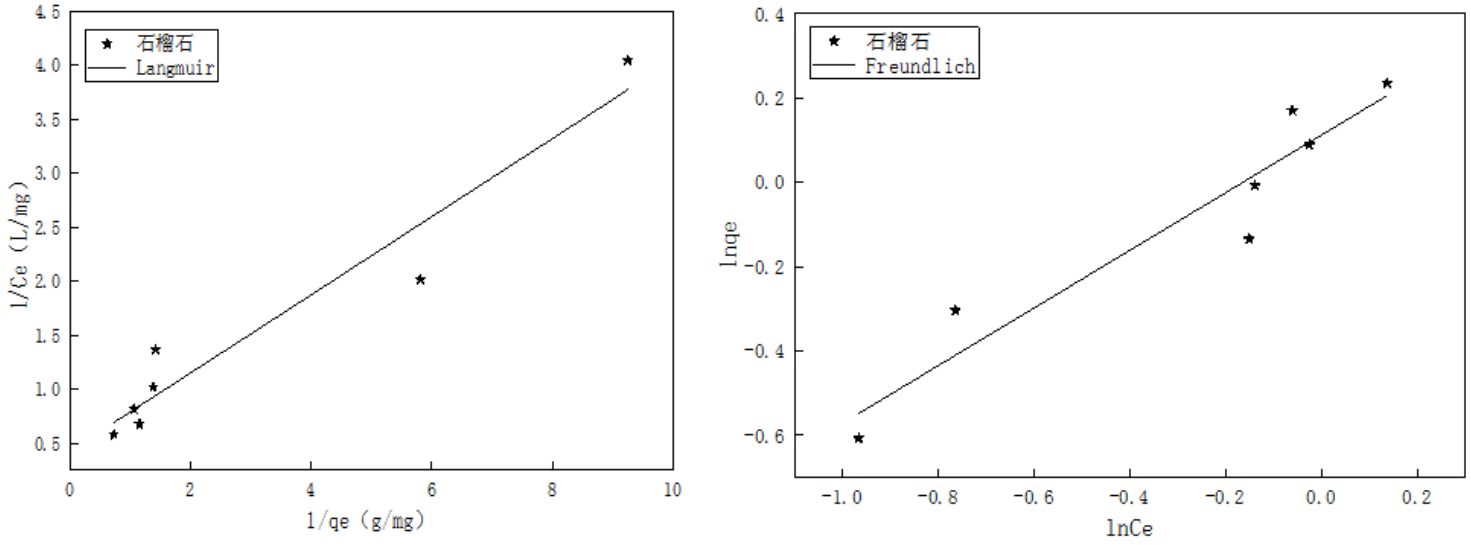

Figure 19

Isotherm adsorption by garnet

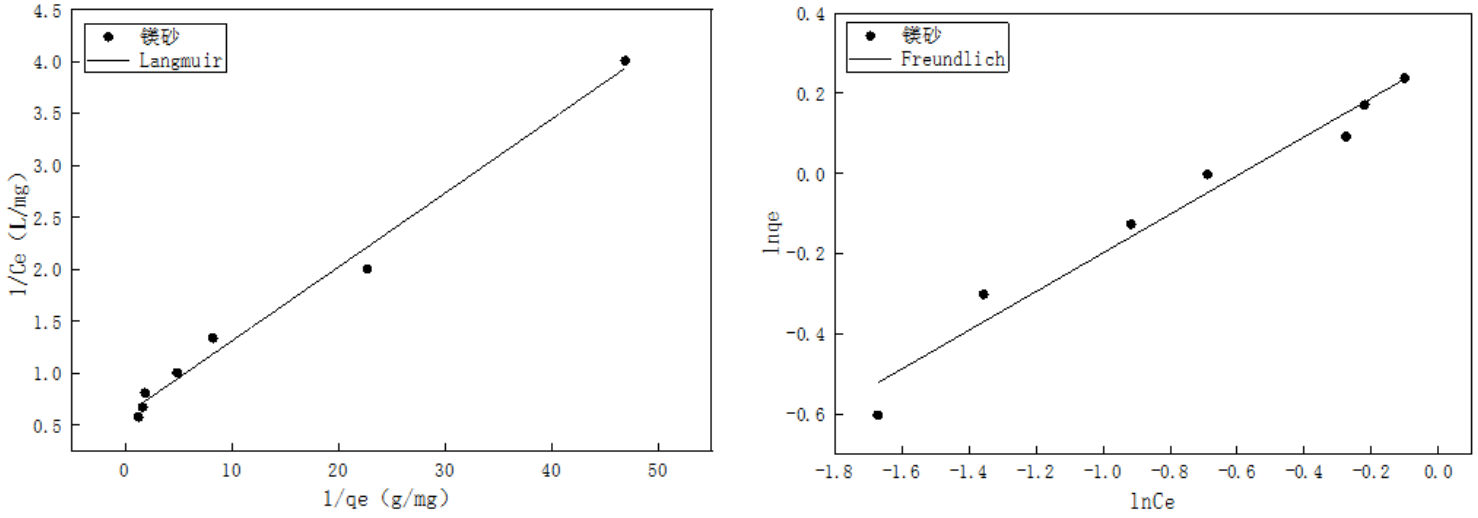

Figure 20

Isotherm adsorption by magnesia